universität wien

MASTERARBEIT / MASTER'S THESIS

Titel der Masterarbeit / Title of the Master's Thesis

„Evolution of Inner Ear Shape in Afrotheria"

verfasst von / submitted by

Fabian Hollinetz BSc

angestrebter akademischer Grad / in partial fulfilment of the requirements for the degree of

Master of Science (MSc)

Wien, 2023 / Vienna 2023

Studienkennzahl lt. Studienblatt / degree programme code as it appears on the student record sheet:	UA 066 220
Studienrichtung lt. Studienblatt / degree programme as it appears on the student record sheet:	Joint-Masterstudium Evolutionary Systems Biology
Betreut von / Supervisor:	Univ.-Prof. Mag. Dr. Philipp Mitteröcker, Privatdoz.
Mitbetreut von / Co-Supervisor:	Anne Le Maître, PhD

Acknowledgements

I want to thank all the people who kindled my interest in living beings from a very young age, including my parents Klaus and Judith, my grandfathers Alfred and Wilhelm as well as my teacher Maria Feichtenschlager.
I want to also extend my gratitude to all the great lecturers at university who helped me shape my views and hone my skills. Those include Univ.-Prof. Mag. Dr. Konrad Fiedler, Univ.-Prof. Mag. Dr. Philipp Mitteröcker, Johannes Jäger, MSc PhD, and Univ.-Prof. Mag. Dr. Mihaela Pavlicev.
I also want to thank the people who guided me through this work. Nicole Grunstra, BA MSc PhD provided materials and greatly helped me in finding the topic and research programme of this thesis. Univ.-Prof. Mag. Dr. Philipp Mitteröcker supervised this thesis and helped with his statistical expertise. Anne Le Maître, PhD helped me improve my coding skills, taught me about anatomy and provided materials. Dr. Guillermo Bravo Morante, MSc provided materials. Dipl.-Biol. Dr. Cathrin Pfaff also provided materials.

Abstract

The mammalian inner ear has seen adaptations to various environmental regimes and multiple evolutionary novelties despite theoretical constraints to its evolvability, mainly tight spatial integration with lots of functionally different components in close proximity and a short developmental timespan. This should lead to less signs of convergent evolution and a greater dependence of shape on phylogeny.
In order to test such predictions, I used methods from geometric morphometrics to compare the inner ear shape of 20 afrotherian species to the shapes of 20 ecologically similar, but only distantly related mammalian species. Shapes were compared via principal component analysis, which showed afrotherian inner ear shapes to be more similar to those of their analogues than to other afrotherian species. Partial least squares analysis was used to find associations between inner ear shape and ecological, locomotor and postural variables. It mainly contrasted aquatic with non-aquatic species in the first component and arboreal versus fossorial species in the second.
This led to the conclusion that ecology is the predominant influencing factor for inner ear shape as opposed to phylogenetic relationships.

Das Innenohr der Säugetiere hat trotz theoretischer Beschränkungen seiner Evolvabilität, insbesondere einer engen räumlichen Integration mit vielen funktionell unterschiedlichen Komponenten in unmittelbarer Nähe zueinander und einer kurzen Entwicklungszeit, Anpassungen an verschiedene Umweltbedingungen und zahlreiche evolutionäre Neuheiten erfahren. Dies sollte zu geringeren Anzeichen konvergenter Evolution und einer stärkeren Abhängigkeit der Form von der Phylogenie führen.
Zur Verifizierung dieser Vorhersagen, verwendete ich Methoden der geometrischen Morphometrie, um die Form des Innenohrs der Säugetiere von 20 Arten Afrotheria mit den Formen von 20 ökologisch ähnlichen, aber nur entfernt verwandten Säugetierarten zu vergleichen. Die Formen wurden mittels Principal Component Analysis verglichen, die zeigte, dass die Innenohrformen der Afrotheria eher denen ihrer Analoga ähnelten als jenen anderer Afrotheria. Partial Least Squares Analysis wurde verwendet, um Zusammenhänge zwischen der Form des Innenohrs und ökologischen, lokomotorischen und Haltungsvariablen zu finden. Sie kontrastierte hauptsächlich aquatische mit nicht-aquatischen Arten in der ersten Komponente und arboreale gegenüber fossorialen Arten in der zweiten Komponente. Daraus ergab sich die Schlussfolgerung, dass die Ökologie, im Gegensatz zu phylogenetischen Beziehungen, der vorherrschende Einflussfaktor auf die Form des Innenohrs ist.

Contents

Introduction

The mammalian inner ear is unique among structures of the vertebrate skeleton in housing functionally different modules in a very close space (Le Maître et al., 2020). It is housed within the bony labyrinth, a caved space within the petrosal bone (Ekdale et al., 2016). Its inferior part consists of the usually spiral shaped cochlea and the saccule of the membranous vestibule, while the superior part of the structure includes the utricle, three semicircular ducts (SCCs) and ampullae (Ekdale et al., 2016). Sensory organs within ampullae of the semicircular canals enable perception of rotational movements of the head, while receptors that respond to linear acceleration are placed within the utricle and saccule (Ekdale et al., 2016). A good sense of posture was likely required during the mammalian radiation due to them adopting a broad range of mobility (Ekdale et al., 2016) (Figure 1). The electro motile outer hair cells embedded in the organ of Corti of the cochlea are a crucial evolutionary novelty originating within the mammalian clade, which enabled the perception of high-frequency sounds, that in turn allowed for the exploitation of a variety of new niches, and the development of new vocalization patterns (Le Maître et al., 2020). The mammalian cochlea evolved to be several times longer than that of birds and other tetrapods, with placentals evolving a high degree of cochlear coiling multiple times independently (Le Maître et al., 2020, Manley, 2012, Ekdale, 2013). Through the development of such evolutionary novelties mammals were able to access a diversity of new ecological niches during their early predominantly nocturnal radiation, a behaviour that made them reliant on hearing (Le Maître et al., 2020).

Evolvability of the Mammalian Inner Ear

The term evolvability has multiple definitions, two notable examples are “the ability of a population to evolve in the direction of selection when stabilizing selection is absent” (Hansen and Houle, 2008); or “the capacity to generate heritable phenotypic variation” (Kirschner and Gerhart, 1998). In the context of this thesis and on a larger scale I would characterize it as a lineage ability to evolve adaptations in the face of shifting ecological regimes.

Among many factors influencing evolvability (see Kirschner and Gerhart, 1998 for a detailed overview), modularity is of particular interest with regards of the inner ear. Structures that serve different functions can be hindered in their capacity to be adapted, if they are in close spatial proximity, or share developmental processes that lead to their formation during embryonic development. This is because the ontogenetic development of an anatomical structure might influence those of other functional components. Thereby, functional adaptations might not emerge, because they would cause a fitness disadvantage in the affected individuals. In a structure as small as the inner ear, developmental integration might not even be needed for this and spatial integration alone might suffice to cause the effect outlined above. Another possible constraint to evolutionary change within the mammalian inner ear is the early cessation of growth in the otic region because cranial differences between many mammals usually form during perinatal and postnatal development (Le Maître et al., 2020).

Despite these theoretical concerns, the history of the evolution of the mammalian inner ear has, as mentioned above, seen many evolutionary innovations and was very likely crucial during the initial radiation of the mammalian clade (Le Maître et al., 2020), which would indicate high selective forces. This gives rise to the question of how the functionally different

and spatially close components of the ear could be adapted seemingly independently to a wide range of functional and environmental regimes (Le Maître et al., 2020).

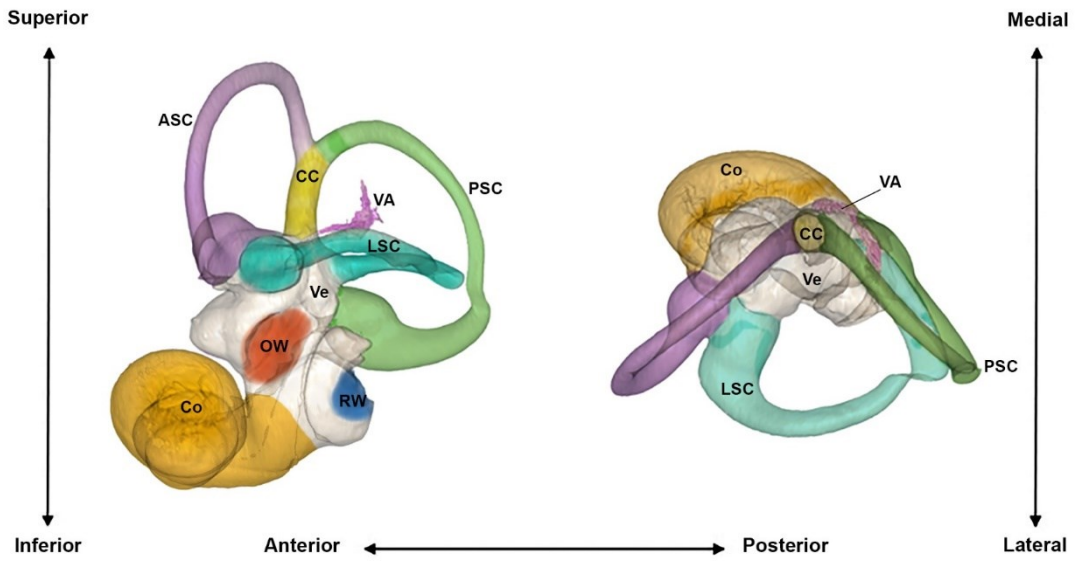

Figure.1: lateral (left) and superior view (right) of the bony labyrinth of *Dendrohyrax arboreus*. Sub structures are labelled and coloured: *ASC*, anterior semicircular canal (purple); *PSC*, posterior semicircular canal (green); *LSC*, lateral semicircular canal (cyan); *CC*, common crus (bright yellow); *VA*, vestibular aqueduct (pink); *Ve*, vestibule (wihte); *OW*, oval window (red); *RW*, round window (blue); *Co*, cochlea (dark yellow)

Afrotheria

Afrotherian mammals were chosen as the main focus of this study because they radiated into a wide range of ecological niches, featuring terrestrial, ground dwelling and aquatic forms. The superorder was recognized relatively recently, and some members of the taxon were previously classified into distantly related groups (Nikaido et al., 2003). Some members of the afrotherian clade show strong resemblance to distantly related mammal groups and occupy similar ecological niches. Hyracoids and proboscideans resemble perissodactyls and artiodactyls, elephant-shrews are adapted for jumping in a similar fashion to lagomorphs (which is why they were initially associated with Glires); golden moles and some tenrecs resemble true moles (Talpidae) and hedge hogs (Erinaceidae) (Tabuce et al., 2008).
A possible relationship between afrotherian mammals was first proposed in a study on α-crystallin protein sequences in elephant, hyrax, aardvark, and elephant shrews (de Jong et al., 1981). The clade was fully recognized based on DNA analysis in the mid-1990s, and those findings were confirmed by multiple molecular and genomic studies (Tabuce et al., 2008)
It is now recognized as one of the big assemblages within placental mammals (Nikaido et al., 2003). The Afrotherian superorder consists of six orders: Proboscidea (elephants), Sirenia (dugongs and manatees), Hyracoidea (hyracoids), Macroscelidea (elephant-shrews), Tubulidentata (aardvarks) and Tenrecoidea (tenrecs and golden moles, also known as ‘‘Afrosoricida’’). They evolved and have been in Africa since the Cretaceous (Tabuce et al., 2008). The Afrotherians long endemic evolution resulting from the physical isolation of the

African continent during the successive breakup events of Gondowanaland (Nikaido et al., 2003), might be an explanation of the mismatch between their molecules and morphology during a process in which afrotherian morphological synapomorphies were supposedly overwritten (Tabuce et al., 2008).

Geometric Morphometrics

The main methods of data collection and statistical analysis employed in this study come from the toolkit of geometric morphometrics. This style of quantitative study of biological shape is a combination of the multivariate analysis of covariance matrices and the direct visualization of shape changes (Bookstein, 1996). It relies on landmark coordinates as basic data input. Landmarks represent biologically or geometrically homologous point locations on an object (Mitteroecker and Schaefer, 2021). Their location is represented by two- or three-dimensional coordinates.

Raw coordinates do not allow for a comparison of shape between landmark sets because the corresponding specimens might differ in size, position, and orientation. These 'nuisance parameters' need to be separated from the shape before being subjected to statistical analysis (Mitteorecker and Gunz, 2009). The method employed in this work is Generalized Procrustes Analysis (GPA; Rohlf and Slice, 1990), which is the most common registration for parametrizing shape in geometric morphometrics (Mitteorecker, 2020). The coordinates are first translated to the same centroid and then scaled to the same centroid size (Mitteroecker and Schaefer, 2021), which is the square root of the summed squared distances between all landmarks and their centroid (Mitteroecker et al., 2013). Lastly the coordinates are rotated in a way that minimizes the summed squared differences between each set of coordinates and the sample average (Mitteroecker and Schaefer, 2021).

In addition to landmarks, many geometric morphometric studies also include semilandmarks, which allow for the geometry of curves or surfaces to be captured.

Since their position cannot be homologized across specimens based on anatomical criteria, they must be estimated in a way that avoids artificial signals in the data resulting from arbitrary placement (Mitteroecker and Schaefer, 2021). To this end their final locations are usually determined by employing the sliding landmark algorithm, which iteratively slides landmarks along their respective curves or surfaces until the shape difference across the sample is minimized (Mitteroecker, 2020). Shape difference can either be quantified by Procrustes distance or by bending energy (Mitteroecker and Schaefer, 2021). Visualization and ease of interpretation is one of the key strengths of geometric morphometrics, because statistical results can be shown as an actual shape or form (Mitteroecker and Schaefer, 2021). Numerous multivariate statistical methods for analysing landmark date exist, those include principal component analysis, multivariate regression, partial least squares analysis, and factor analysis (Mitteroecker and Schaefer, 2021). Among those principal component analysis and two block partial least squares analysis were used for statistical analysis in this study. Principal component analysis (PCA) is an ordination technique, and as such a low dimensional representation of multivariate differences between specimens (Mitteroecker, 2020). I used it to visualize shape difference between specimens as two dimensional scatterplots.

Two-block partial least squares (PLS) was invented by Herman Wold (Mitteroecker, 2012). It is similar to principal component analysis, but works on two separate sets of date, called blocks. The algorithm looks for a linear combination for each block so that the covariance between those two linear combinations is maximized (Rohlf and Corti, 2000). It thereby

allows for both landmark data and associated contextual variables to be treated in a multivariate way (Mitteroecker and Schaefer, 2021). In this work, partial least squares analysis was used to find connections between species ecology and inner ear shape.

Research Question

The main research question of this thesis is whether the shapes of functionally different components within the inner ear can respond differentially to evolutionary forces and evolve independently from each other, or if they are more influenced by phylogenetic relationships. To this end I analysed the inner ear shape of 40 different mammalian species. Roughly half of the sample consisted of species from the afrotherian clade, while the other half included analogous species from other mammal groups. Signs of convergent evolution within the inner ear could point to the structure being more responsive to ecological regimes, whereas strong similarity within afrotherians would point at strong dependence of shape on phylogeny thereby indicating low evolvability.

Materials and Methods

Sample composition

The final sample contained 20 afrotherian species and 20 species from analogous mammal groups. Table 1 gives an overview of the sample composition.

Afrotherian species	Common name	Analog
Amblysomus hottentotus, *Chrysochloris asiatica*	golden moles	*Cryptomys hottentotus*, *Talpa europaea*
Dendrohyrax arboreus	tree hyrax	*Tamandua mexicana*
Heterohyrax brucei, *Procavia capensis*	more terrestrial hyraxes	*Marmota marmota*, *Ochotona rufescens*
Dugong dugon, *Trichechus* sp.	sea cows	*Odobenus rosmarus*, *Phoca vitulina*, *Sotalia fluviatilis*
Elephantulus rufescens *Elephantulus rupestris* *Macroscelides proboscideus*	small-bodied elephant shrews or sengis	*Microtus arvalis*, *Mus musculus*, *Rattus rattus*, *Sorex araneus*
Petrodromus tetradactylus *Rhynchocyon cirnei*	larger-bodied sengis	*Oryctolagus cuniculus*, *Rattus rattus*, *Tragulus javanicus*
Elephas maximus	elephant	none
Hemicentetes semispinosus *Setifer setosus* *Tenrec ecaudatus*	hedgehog-like tenrecs	*Erinaceus europaeus*
Limnogale mergulus	shrew-like tenrecs	*Sorex araneus*
Orizoryctes tetradactyla	mole-like tenrec	*Talpa europaea*
Orycteropus afer	aardvark	*Manis tricuspis*, *Tamandua mexicana*, *Tolypeutes matacus*
Potamogale velox	otter shrew	*Lutra lutra*, *Ornithorhynchus anatinus*

Table 1: Sample composition. Afrotherian species are shown along with species chosen as analogues.

Afrotherian taxa were selected to cover a broad range of ecological niches. Analogues were also selected to cover a wide phylogenetic range (Figure3).

Data

Computer tomography (CT) scans of adult crania, except for the elephant where a juvenile was used due to size, were used as the main source of raw data for this work. Sexual dimorphism in the inner ear exists but is small enough to be neglected (Gonzales et al., 2019).
CT scans were produced at the scanning facilities of the departments of Evolutionary Biology and Palaeontology at the University of Vienna and at the Natural History Museum of Vienna, others were downloaded from MorphoSource (see Appendix for more detailed information).

Landmarking

After segmentation, which is the process by which 3D models are obtained from raw CT scans, 13 landmarks and 111 semilandmarks were placed on the 3D shapes of the specimen's bony labyrinth according to a slightly modified landmarking scheme taken from Gunz et al. (2012).
The landmark definitions are listed in Table 2. Semilandmarks were placed on the midlines of the semicircular canals and the cochlea as well as at the outline of the oval window. Figure 2 shows a fully landmarked specimen (*Tragulus javanicus*).

Nr.	Definition
Landmarks	
1	ASC ampulla to vestibule
2	ASC ampulla to slender part of ASC
3	CCR to ASC & PSC
4	CCR to vestibule
5	Slender part of PSC to ampulla
6	PSC ampulla to vestibule
7	Slender part of LSC to vestibule
8	Slender part of LSC to ampulla
9	LSC ampulla to vestibule
10	Helicotrema
11	Centre of the round window
12	Posterior extremity of the axis of max elongation of the oval window
13	Anterior extremity of the axis of max elongation of the oval window
Semilandmarks	
1 - 20	Midline curve of the ASC
21 - 40	Midline curve of the PSC
41 - 45	Midline curve of the CCR
46 - 65	Midline curve of the LSC
66-105	Midline curve of the cochlea
106-111	Outline of the oval window

Table 2: Definition of landmarks and semilandmarks

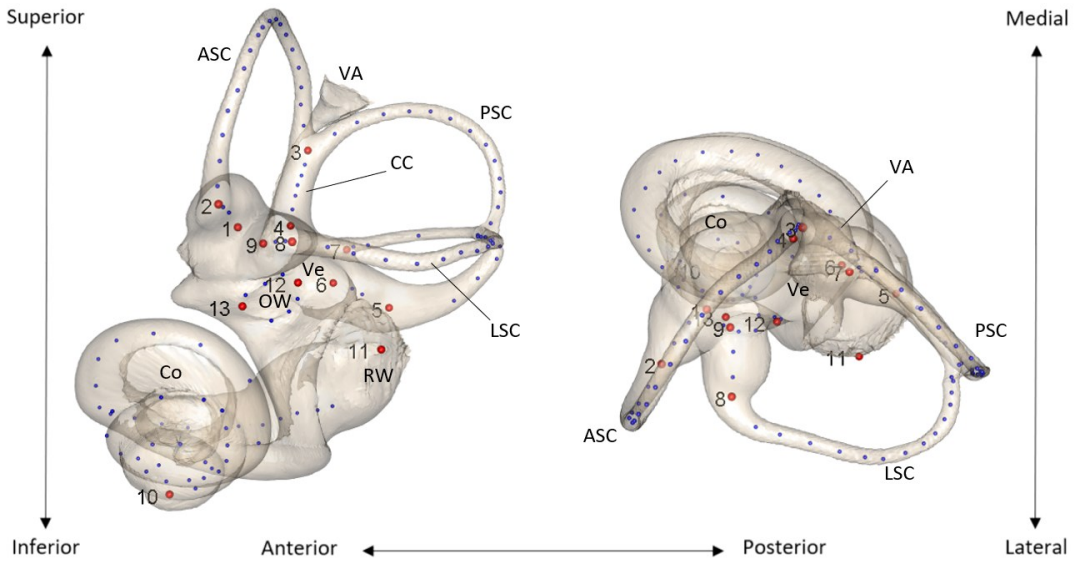

Figure 2: Fully landmarked CT scan of *Tragulus Javanicus*, both in lateral (left) and superior view (right). Landmarking was carried out according to a slightly modified landmarking scheme taken from Gunz et al. (2012). Anatomical Landmarks are displayed in red and are numbered, semilandmarks are displayed in blue. 13 anatomical landmarks are defined. 20 semilandmarks were placed on the midline of each semicircular canal, 5 were placed on the common crus, 40 on the midline of the cochlea and six on the outline of the oval window. *ASC*, anterior semicircular canal; *PSC*, posterior semicircular canal; *LSC*, lateral semicircular canal; *CC*, common crus; *VA*, vestibular aqueduct; *Ve*, vestibule; *OW*, oval window; *RW*, round window; *Co*, cochlea

Contextual Data

Contextual data on all species in the sample was taken from PanTHERIA (Jones et al., 2009), Spoor et al. (2007), Silcox et al. (2009), Cox and Jeffery (2010) as well as from the *Handbook of the Mammals of the world* (Wilson et al, 2009).
The data contains information on body mass, pursuit of moving prey, degree of aquatic lifestyle, degree of arboreal lifestyle, degree of ground dwelling lifestyle, scansorial locomotion, cursorial locomotion, ability to leap and jump, fossorial locomotion, three-dimensional movement, agility, and degree of orthogrady vs. pronogrady. All variables except body mass were measured on an ordinal scale. Tab.3 gives an overview of all contextual variables, their scale as well as their range.

Variable	Scale	Range
Body Mass	interval	9.18 – 3269794 (g)
Pursue moving prey	ordinal	1 - 3
Aquatic	ordinal	1 - 4
Arboreal	ordinal	1 - 3
Terrestrial ground dwelling	ordinal	1 - 3
Scansorial	ordinal	1 - 3
Cursorial	ordinal	1 - 2
Leaping jumping hopping	ordinal	1 - 3
Fossorial	ordinal	1 - 3
3d movement	ordinal	1 - 3
Agility	ordinal	1 - 6
Orthogrady vs pronogrady	ordinal	3 - 5

Tab. 3 Contextual variables together with their scale and range. All variables except body mass were measured on an ordinal scale. For the ordinal variables 1 corresponds to a low score.

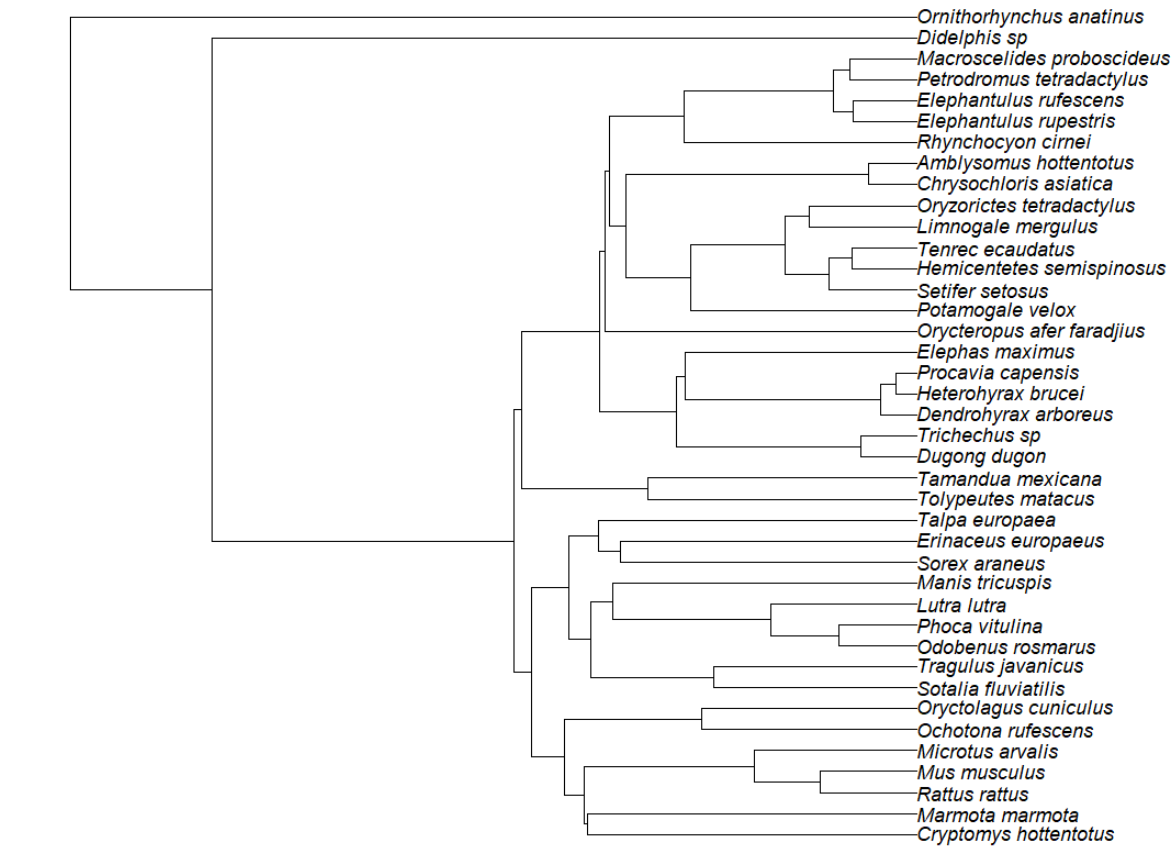

Figure3: Ultrametric tree showing the phylogenetic relationship between the species in the sample

Statistical Analysis

Landmark data from specimens where the scan of the bony labyrinth was taken from the left side of the head was mirrored.
Since *Amblysomus hottentotus* and *Amblysomus iris* were recognized as one species during the time of the analysis, a mean shape was calculated out of their respective landmark data and used under the name *Amblysomus hottentotus* during further analysis.

Procrustes superimposition was used to create comparable shape coordinates by aligning, rotating, and scaling them. A mean shape was computed and each specimens Procrustes distance from the mean shape was computed in order to find outliers.

The Procrustes coordinates were then analysed with principal component analysis. Shape prediction was employed to find shape features corresponding to the main principal components.

In order to quantify allometric effects a linear regression of logarithmic body mass on Procrustes coordinates was performed.

Partial least squares (PLS) analysis was employed to find covariation between ecological data and shape variables. The first variable block for the PLS contained the superimposed landmark data, the second contained z-transformed contextual variables.

Software

Landmarking was carried out in Amira (Thermo Fisher Scientific, 2022). Statistical analysis was carried out in Rstudio (Rstudio Team, 2022) using R (R core Team, 2021). This included the use of the packages ape version 5.6-2 (Paradis and Schliep, 2019), geomorph (Baken et al., 2021; Adams et al., 2022), geomorph version 4.0.4 (Schlager, 2017), phytools version 1.0-3 (Revell, 2012), rgl version 0.109.6 (Murdoch and Adler, 2022), jpeg version 0.1-9 (Urbanek, 2021), pls version 2.8-1 (Liland et al., 2022), picante version 1.8.2 (Kembel et al., 2021), adephylo version 1.1-11 (Jombart and Dray, 2009), ade4 version 1.7-19 (Dray and Dufour, 2007; Bougeard and Dray, 2018; Chessel et al., 2004, Dray et al., 2007; Thioulouse et al., 2018), phylobase version 0.8.10 (Hackathon et al., 2020), geiger version 2.0.10 (Pennell et al., 2014), caper version 1.0.1 (Orme et al., 2018), readxl version 1.4.0 (Wickham and Bryan, 2022), openxlsx version 4.2.5 (Schauberger and Walker, 2021), knitr version 1.39 (Yihui Xie, 2022), ggplot2 version 3.3.6 (Wickham, 2016), ggrepel version 0.9.1 (Slowikowski, 2021), and forcats version 0.5.2 (Wickham, 2022).

Materials and Methods

Outliers

The distance plot in Figure4 shows that the aquatic species (*Sotalia fluvitalis*, *Dugong dugon*) separate the most from the rest. Compared to the other specimen their semicircular canal size relative to the size of the cochlea is considerably smaller than in the rest of the sample.

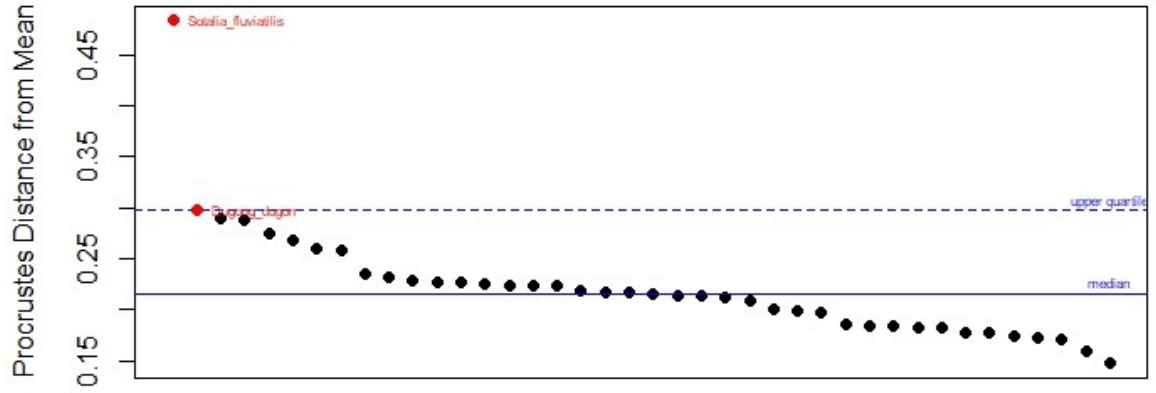

Figure 4: This plot shows the specimens Procrustes distance from the mean shape. Outliers are plotted in red and labelled.

Principal Component Analysis

The scree plot visualizing the explained variance of the principal components (Figure 5) featured a drop off in explanatory power after the 5th component. The first six were therefore examined more closely.

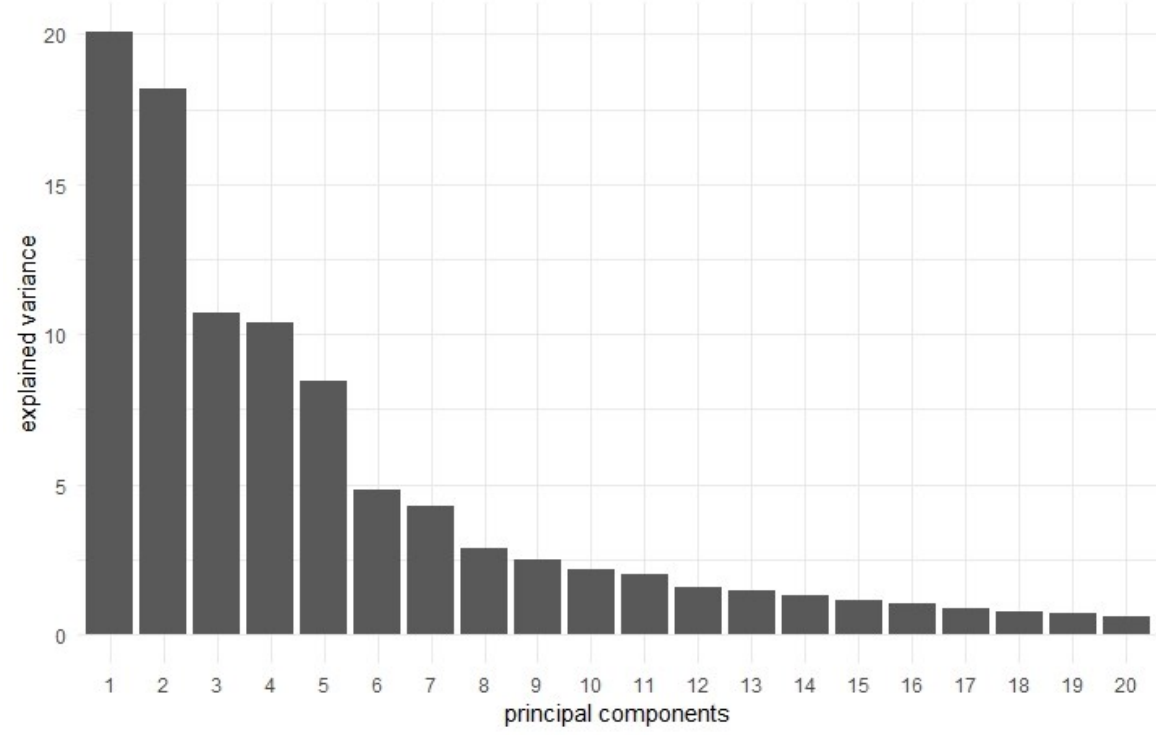

Figure 5: Scree plot displaying the explained variance in per cent of the total variance for the first 20 principal components

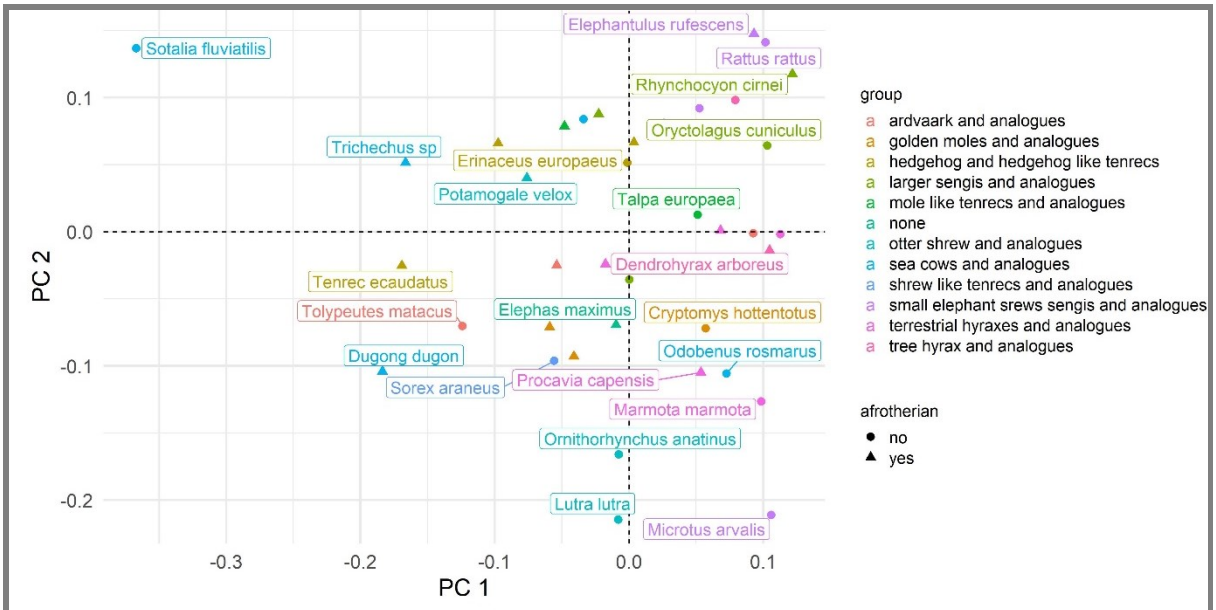

Figure 6: Scatterplot plotting each of the specimens' score on PC 1 and PC 2 against each other. Afrotherians are displayed as triangles, analogues are displayed as rounds. The specimens were divided into ecological guilds and coloured accordingly.

Figure 6 visualizes the specimens scores for the first two principal components. Specimens with a high score in principal component one (Figure 7) feature large semicircular canals in relation to cochlea size. The cochlea is short and narrow, especially towards the end. Specimen with a low value for principal component 1 (Figure 8) have smaller semicircular canals and an especially wide cochlea. Their vestibule is enlarged. Principal component two features species with a wider, lesser coiled cochlea on the apex (Figure 9), and specimens with a relatively narrow, yet strongly coiled cochlea on the base (Figure 10). *Sotalia fluvitalis*, which also is the strongest outlier (Figure 4) of the sample and is placed on the top left here, has an especially large and uncoiled cochlea and very small semicircular canals relative to cochlea size. Despite some overlap, aquatic mammals (sea cows and analogues), small elephant shrews, sengis and analogues, golden moles, and analogues as well as otter shrews and analogues seem to be separated well by principal component one and two. Note that the walrus (*Odobenus rosmarus*) falls out of the aquatic group. Compared to the other aquatic mammals its inner ear is close to the average shape in structure but with a larger circumference of the semicircular canals and the cochlea, which is variation that is not captured by the landmarking scheme. Interestingly there seems to be no clustering of afrotherians against non-afrotherians, but it can be observed that afrotherian tend to have a more central position within the plot.

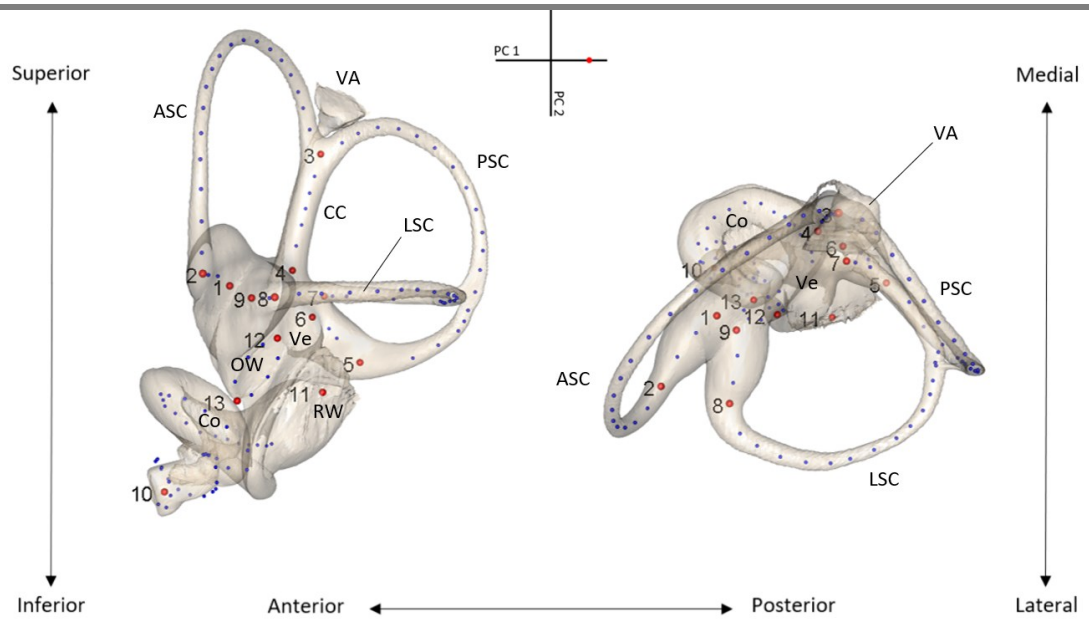

Figure 7: Predicted shape configuration of a specimen with a high PC 1 score and an average score on PC 2 in both lateral (left) and superior (right) view. Landmarks are displayed in red and are numbered, semilandmarks are displayed in blue. *ASC*, anterior semicircular canal; *PSC*, posterior semicircular canal; *LSC*, lateral semicircular canal; *CC*, common crus; *VA*, vestibular aqueduct; *Ve*, vestibule; *OW*, oval window; *RW*, round window; *Co*, cochlea; Note that the shape is a prediction based on predicted landmark position and is just shown to aid visualization.

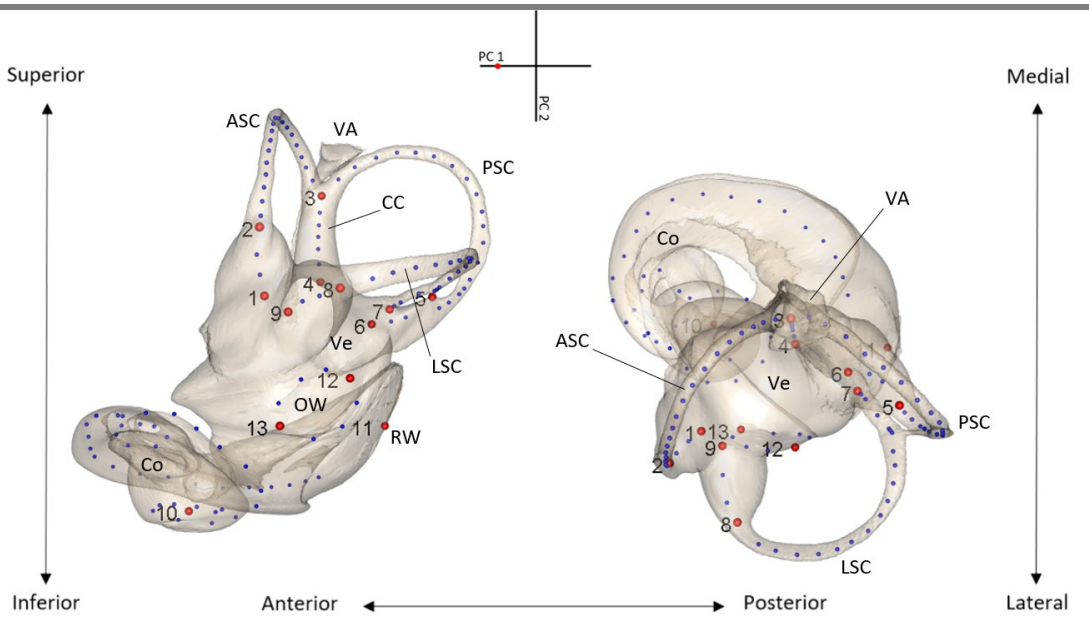

Figure 8: Predicted shape configuration of a specimen with a low PC 1 score and an average score on PC 2 in both lateral (left) and superior (right) view. Landmarks are displayed in red and are numbered, semilandmarks are displayed in blue. *ASC*, anterior semicircular canal; *PSC*, posterior semicircular canal; *LSC*, lateral semicircular canal; *CC*, common crus; *VA*, vestibular aqueduct; *Ve*, vestibule; *OW*, oval window; *RW*, round window; *Co*, cochlea; Note that the shape is a prediction based on predicted landmark position and is just shown to aid visualization.

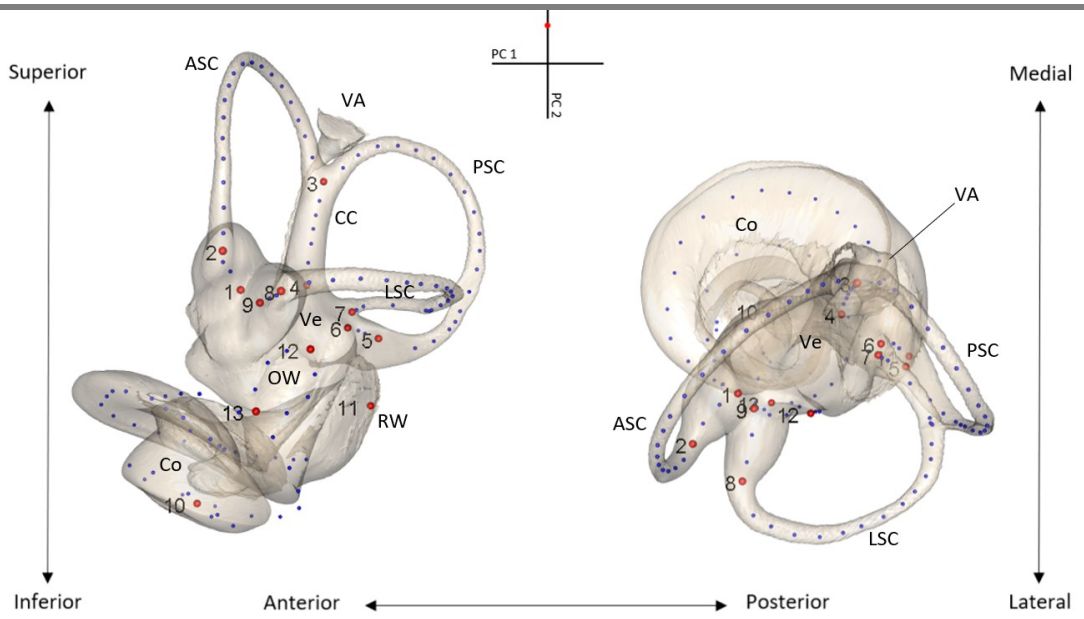

Figure 9: Predicted shape configuration of a specimen with a high PC 2 score and an average score on PC 1 in both lateral (left) and superior (right) view. Landmarks are displayed in red and are numbered, semilandmarks are displayed in blue. *ASC*, anterior semicircular canal; *PSC*, posterior semicircular canal; *LSC*, lateral semicircular canal; *CC*, common crus; *VA*, vestibular aqueduct; *Ve*, vestibule; *OW*, oval window; *RW*, round window; *Co*, cochlea; Note that the shape is a prediction based on predicted landmark position and is just shown to aid visualization.

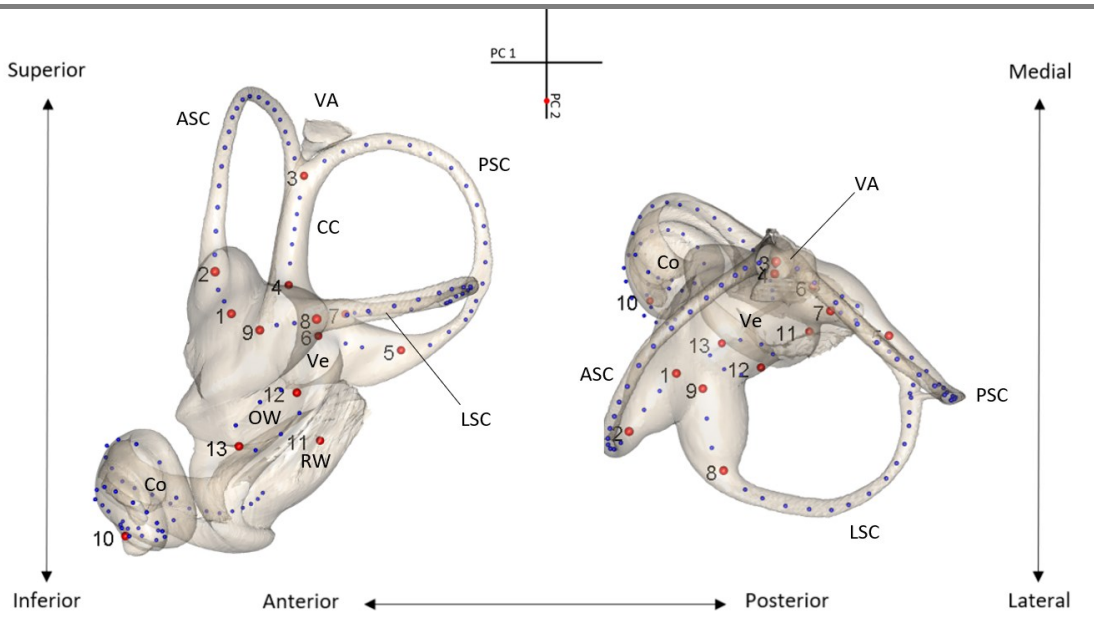

Figure 10: Predicted shape configuration of a specimen with a low PC 2 score and an average score on PC 1 in both lateral (left) and superior (right) view. Landmarks are displayed in red and are numbered, semilandmarks are displayed in blue. *ASC*, anterior semicircular canal; *PSC*, posterior semicircular canal; *LSC*, lateral semicircular canal; *CC*, common crus; *VA*, vestibular aqueduct; *Ve*, vestibule; *OW*, oval window; *RW*, round window; *Co*, cochlea; Note that the shape is a prediction based on predicted landmark position and is just shown to aid visualization.

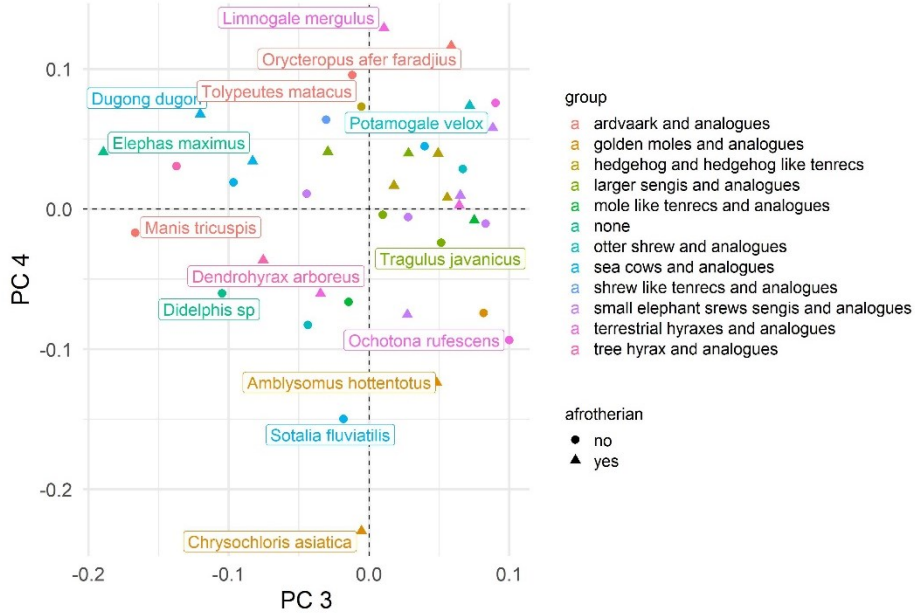

Figure 11: Scatterplot plotting each specimens' score on PC 3 and PC 4 against each other. Afrotherians are displayed as triangles, analogues are displayed as dots. The specimens were divided into ecological guilds and coloured accordingly.

Figure 11 visualizes the specimens' scores for principal component three and four. Specimens with a high score along principal component three (Figure 12) are characterized by a large semicircular canal size when compared to cochlea size. The cochlea itself is wide, flat, and strongly coiled.

Specimens with a low value for principal component three (Figure 14) have an elongated cochlea that tapers towards the end and is strongly coiled. The semicircular canals are relatively small. Principal component four are characterized by a species with a large cochlea that taper equally and is strongly coiled on the top (Figure 13). Specimens with low principal component four scores (Figure15) have a short, wide, uncoiled cochlea. Despite some overlap, golden moles and analouges, tree hyraxes and analouges, sea cows and analogues cluster in the space of the third and fourth principal component (Figure 11).

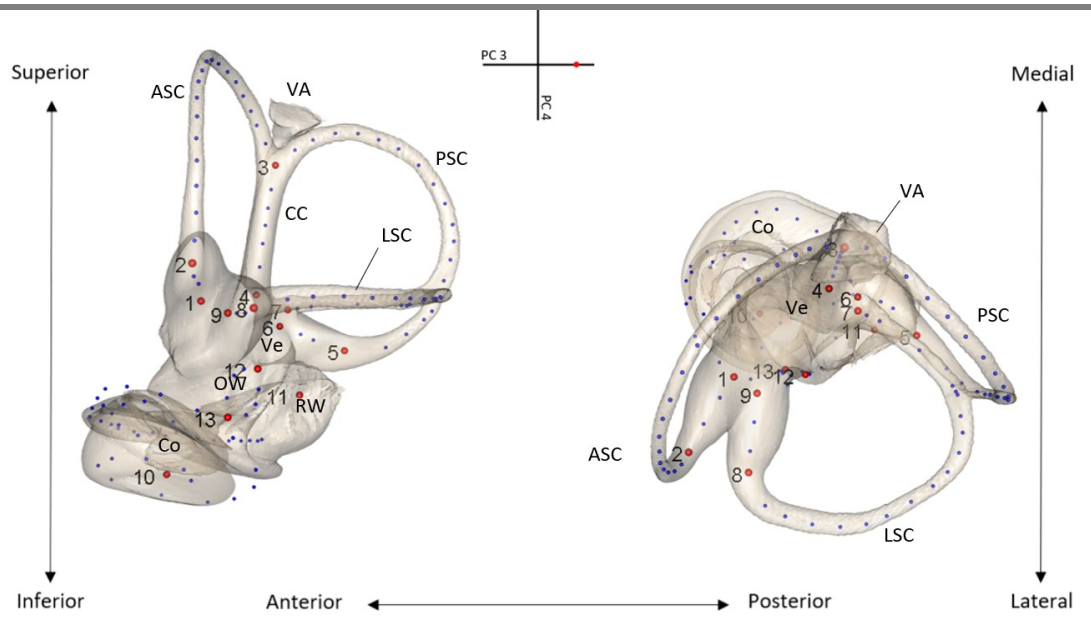

Figure 12: Predicted shape configuration of a specimen with a high PC 3 score and an average score on PC 4 in both lateral (left) and superior (right) view. Landmarks are displayed in red and are numbered, semilandmarks are displayed in blue. *ASC*, anterior semicircular canal; *PSC*, posterior semicircular canal; *LSC*, lateral semicircular canal; *CC*, common crus; *VA*, vestibular aqueduct; *Ve*, vestibule; *OW*, oval window; *RW*, round window; *Co*, cochlea; Note that the shape is a prediction based on predicted landmark position and is just shown to aid visualization.

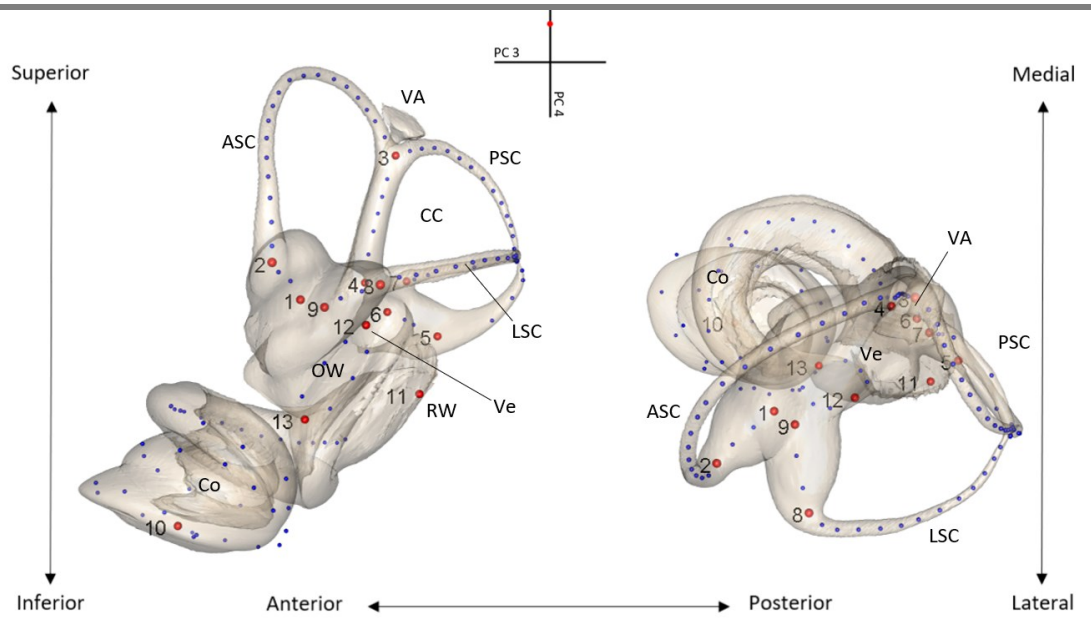

Figure 13: Predicted shape configuration of a specimen with a high PC 4 score and an average score on PC 3 in both lateral (left) and superior (right) view. Landmarks are displayed in red and are numbered, semilandmarks are displayed in blue. *ASC*, anterior semicircular canal; *PSC*, posterior semicircular canal; *LSC*, lateral semicircular canal; *CC*, common crus; *VA*, vestibular aqueduct; *Ve*, vestibule; *OW*, oval window; *RW*, round window; *Co*, cochlea; Note that the shape is a prediction based on predicted landmark position and is just shown to aid visualization.

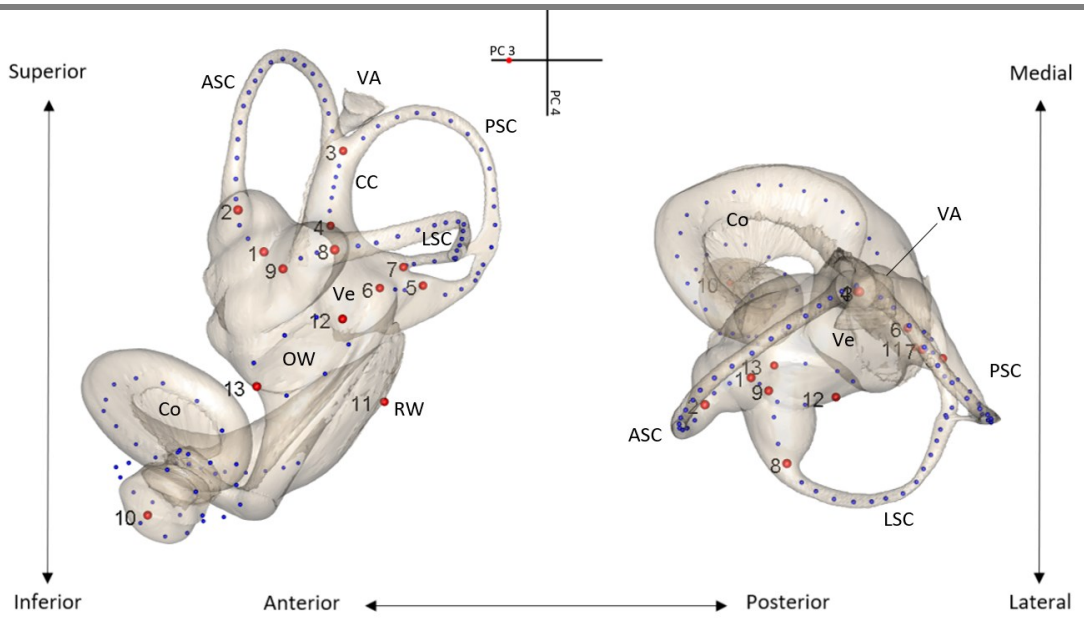

Figure 14: Predicted shape configuration of a specimen with a low PC 3 score and an average score on PC 4 in both lateral (left) and superior (right) view. Landmarks are displayed in red and are numbered, semilandmarks are displayed in blue. *ASC*, anterior semicircular canal; *PSC*, posterior semicircular canal; *LSC*, lateral semicircular canal; *CC*, common crus; *VA*, vestibular aqueduct; *Ve*, vestibule; *OW*, oval window; *RW*, round window; *Co*, cochlea; Note that the shape is a prediction based on predicted landmark position and is just shown to aid visualization.

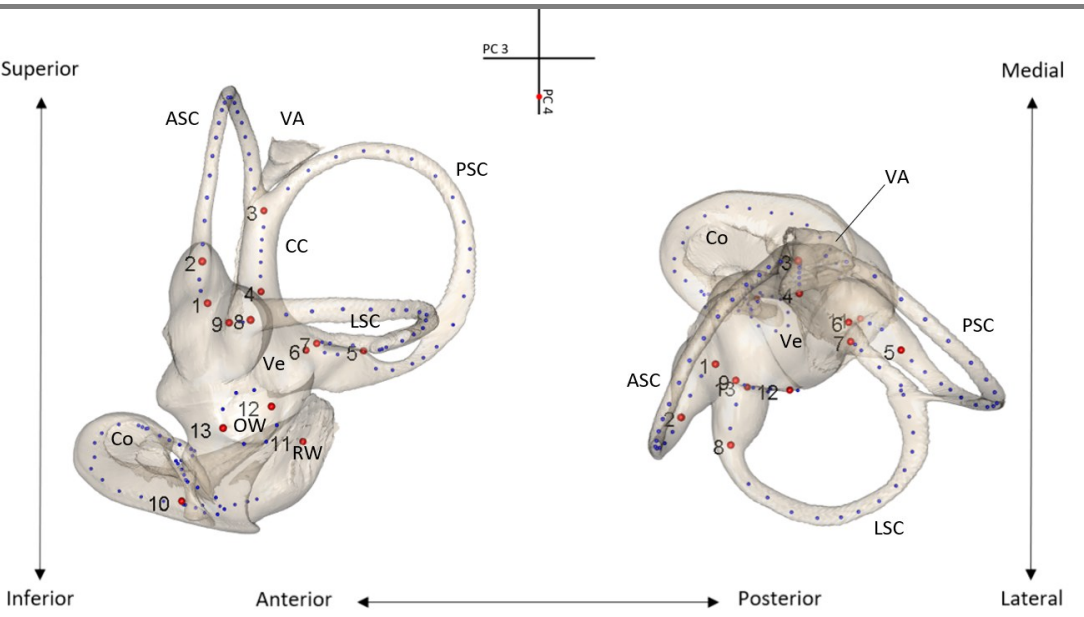

Figure 15: Predicted shape configuration of a specimen with a low PC 4 score and an average score on PC 3 in both lateral (left) and superior (right) view. Landmarks are displayed in red and are numbered, semilandmarks are displayed in blue. *ASC*, anterior semicircular canal; *PSC*, posterior semicircular canal; *LSC*, lateral semicircular canal; *CC*, common crus; *VA*, vestibular aqueduct; *Ve*, vestibule; *OW*, oval window; *RW*, round window; *Co*, cochlea; Note that the shape is a prediction based on predicted landmark position and is just shown to aid visualization.

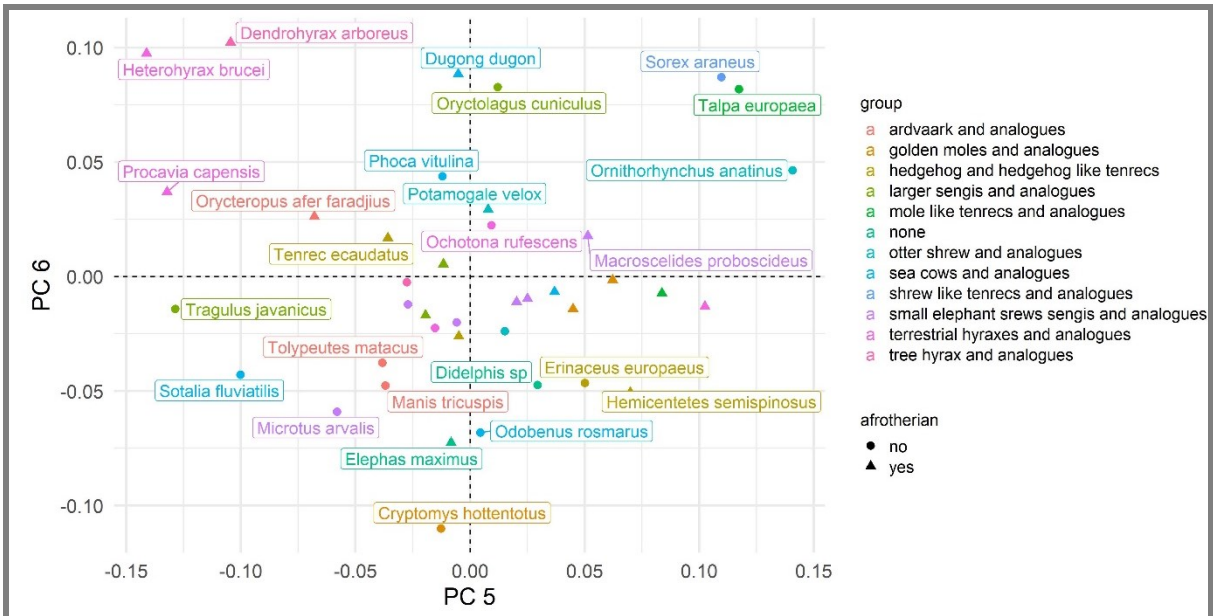

Figure 16: Scatterplot plotting each specimens' score on PC 5 and PC 6 against each other. Afrotherians are displayed as triangles, analogues are displayed as dots. The specimens were divided into ecological guilds and coloured accordingly.

Figure 16 visualizes the specimens scores for principal component five and six.
Specimens with a high score along principal component five (Figure 17) are characterized by a long and wide cochlea with an elongated base. The semicircular canals appear wider on the anterior-posterior axis. Specimen with a low value for principal component five (Figure 19) have a shortened, strongly coiled cochlea and semicircular canals that extend more along the superior-inferior axis. The cochlea is short, strongly coiled, and tapers towards the end.
Principal component six are characterized by a species with large semicircular canals and a short, flat cochlea on the top (Figure 18). Specimens with low principal component six scores (Figure 20) have small semicircular canals and their cochlea features an especially prominent inferior taper.

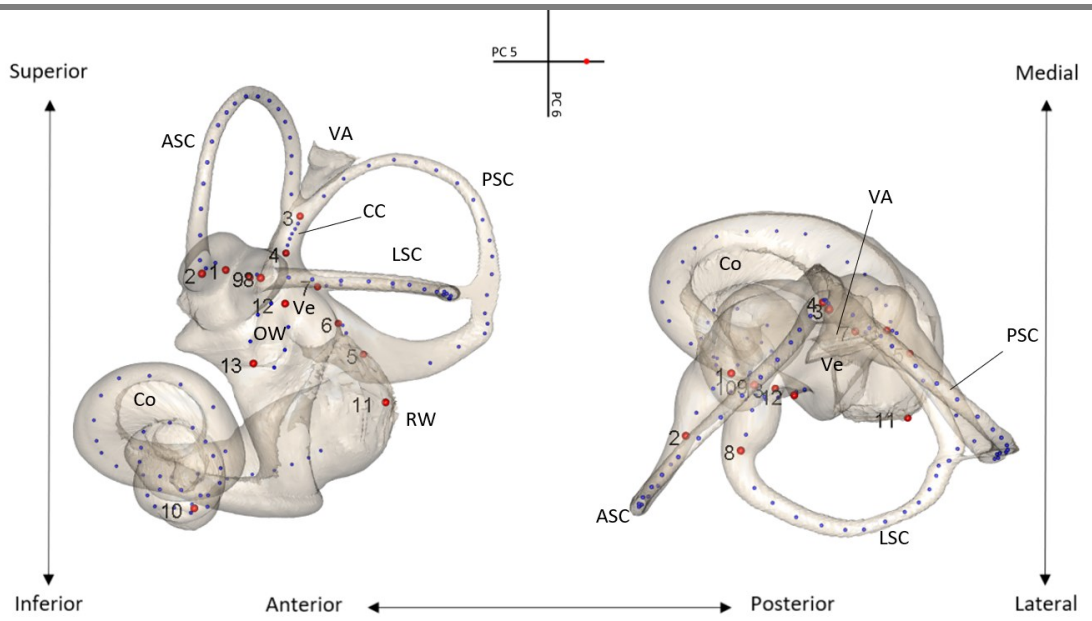

Figure 17: Predicted shape configuration of a specimen with a high PC 5 score and an average score on PC 6 in both lateral (left) and superior (right) view. Landmarks are displayed in red and are numbered, semilandmarks are displayed in blue. *ASC*, anterior semicircular canal; *PSC*, posterior semicircular canal; *LSC*, lateral semicircular canal; *CC*, common crus; *VA*, vestibular aqueduct; *Ve*, vestibule; *OW*, oval window; *RW*, round window; *Co*, cochlea; Note that the shape is a prediction based on predicted landmark position and is just shown to aid visualization.

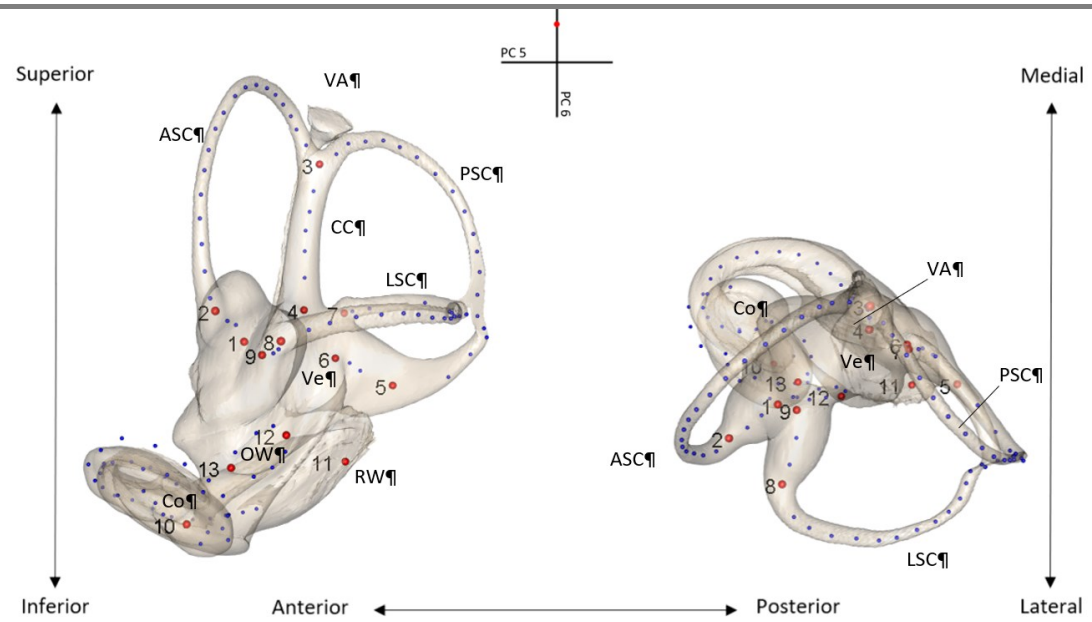

Figure 18: Predicted shape configuration of a specimen with a high PC 6 score and an average score on PC 5 in both lateral (left) and superior (right) view. Landmarks are displayed in red and are numbered, semilandmarks are displayed in blue. *ASC*, anterior semicircular canal; *PSC*, posterior semicircular canal; *LSC*, lateral semicircular canal; *CC*, common crus; *VA*, vestibular aqueduct; *Ve*, vestibule; *OW*, oval window; *RW*, round window; *Co*, cochlea; Note that the shape is a prediction based on predicted landmark position and is just shown to aid visualization.

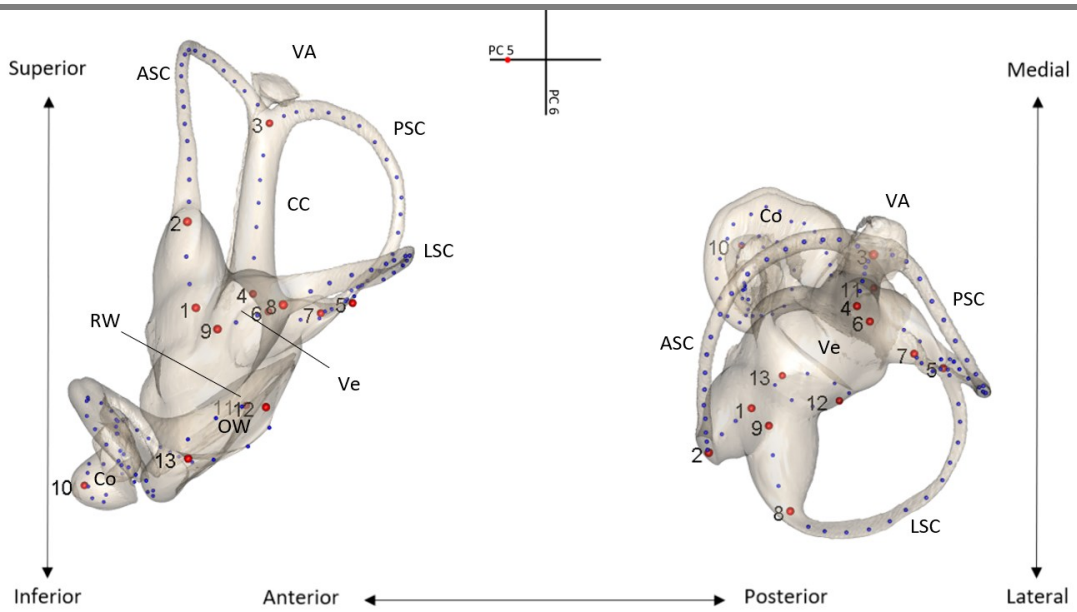

Figure 19: Predicted shape configuration of a specimen with a low PC 5 score and an average score on PC 6 in both lateral (left) and superior (right) view. Landmarks are displayed in red and are numbered, semilandmarks are displayed in blue. *ASC*, anterior semicircular canal; *PSC*, posterior semicircular canal; *LSC*, lateral semicircular canal; *CC*, common crus; *VA*, vestibular aqueduct; *Ve*, vestibule; *OW*, oval window; *RW*, round window; *Co*, cochlea; Note that the shape is a prediction based on predicted landmark position and is just shown to aid visualization.

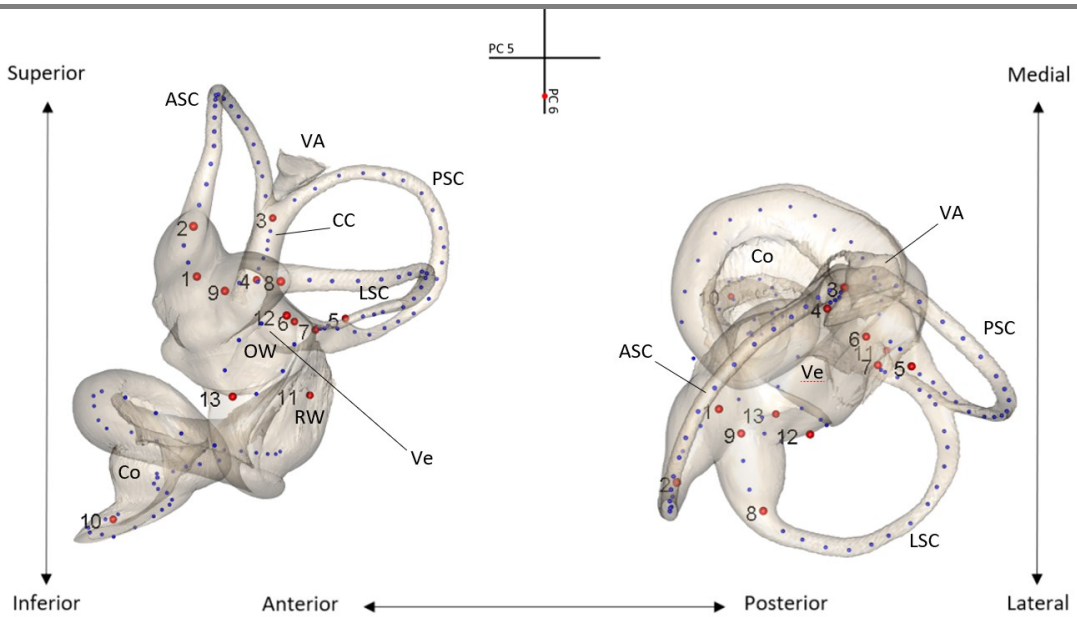

Figure 20: Predicted shape configuration of a specimen with a low PC 6 score and an average score on PC 5 in both lateral (left) and superior (right) view. Landmarks are displayed in red and are numbered, semilandmarks are displayed in blue. *ASC*, anterior semicircular canal; *PSC*, posterior semicircular canal; *LSC*, lateral semicircular canal; *CC*, common crus; *VA*, vestibular aqueduct; *Ve*, vestibule; *OW*, oval window; *RW*, round window; *Co*, cochlea; Note that the shape is a prediction based on predicted landmark position and is just shown to aid visualization.

Allometry

Procrustes shape coordinates showed a weak yet significant association with body mass (R^2 = 0.072; F = 2.99; p = 0.001). Figure 21 shows a scatterplot of the common allometric component (CAC) against the first residual shape component (RSC1) for each specimen. Figure 22 displays CAC against logarithmic body mass.

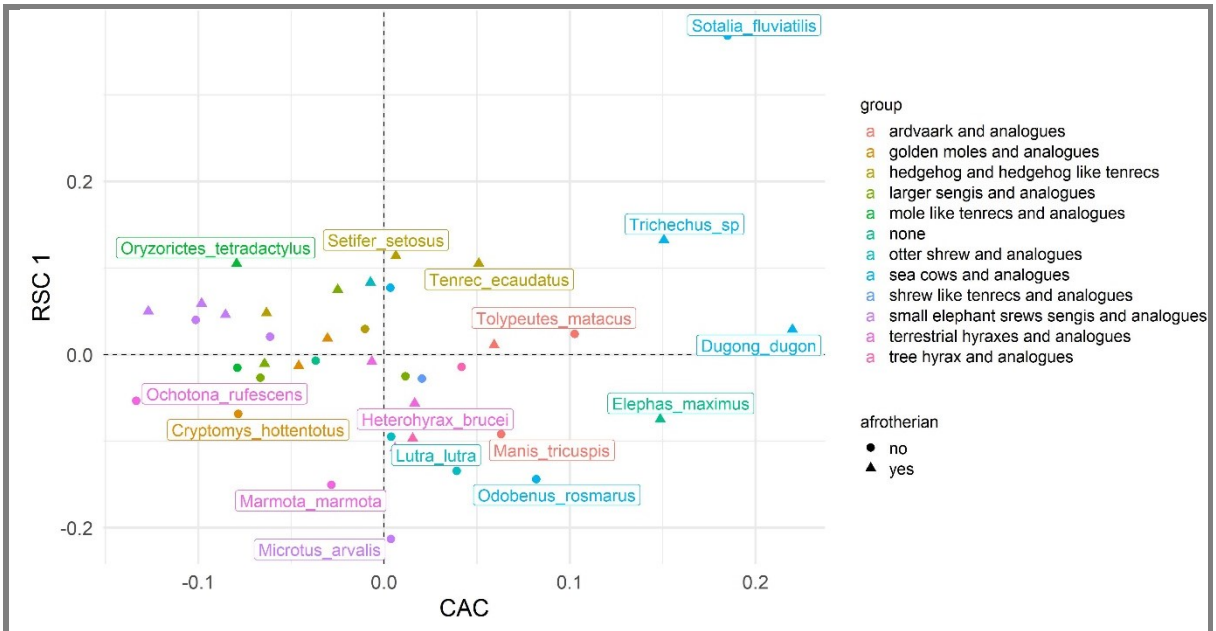

Figure 21: common allometric component (CAC) plotted against the first residual shape component (RSC1) for each specimen. Afrotherians are displayed as triangles, analogues are displayed as dots. The specimens were divided into ecological guilds and coloured accordingly.

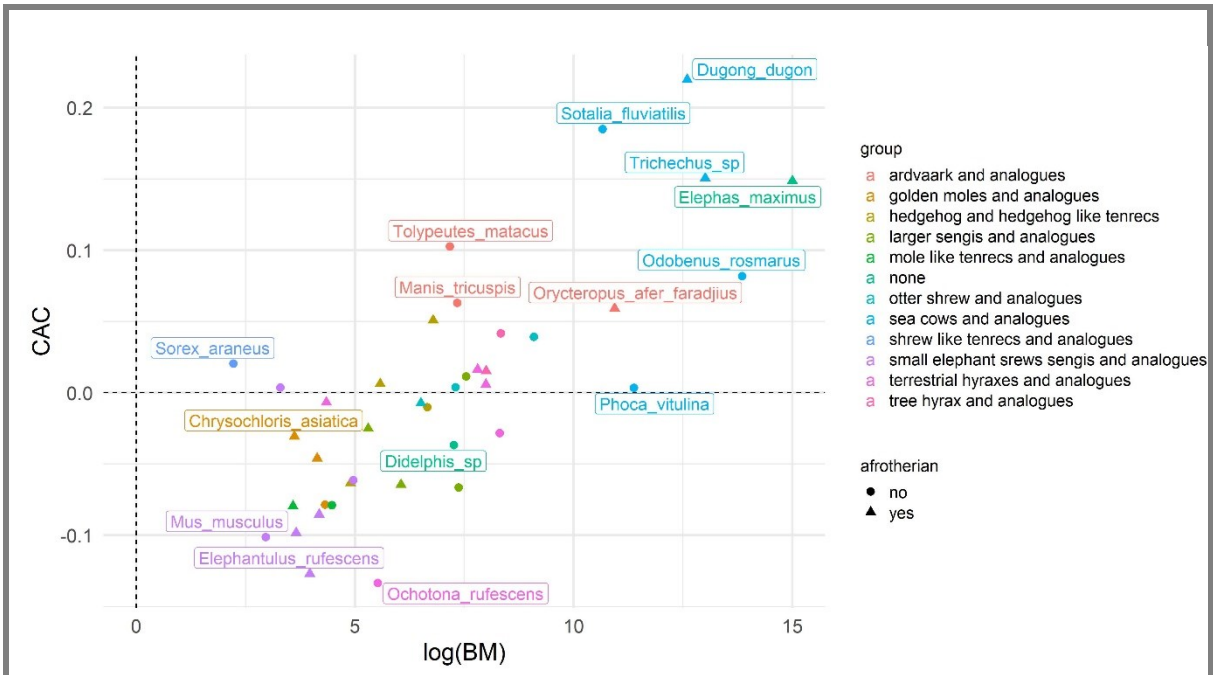

Figure 22: scatterplot plotting each specimen's logarithmic body mass and common allometric component (CAC) against each other. Afrotherians are displayed as triangles, analogues are displayed as dots. The specimens were divided into ecological guilds and coloured accordingly.

Partial Least Squares Analysis

The *p*-values for the first three PLS dimensions (Tab.4) show that the first two levels capture a significant association between ear shape and the contextual variables. The third one should be viewed with a more critical eye; it might contain biologically meaningful information but might also have captured measurement errors or random variation.

SW	P
1	0.000999001
2	0.00599401
3	0.0959041

Tab.4: *p*-values for the first three PLS components

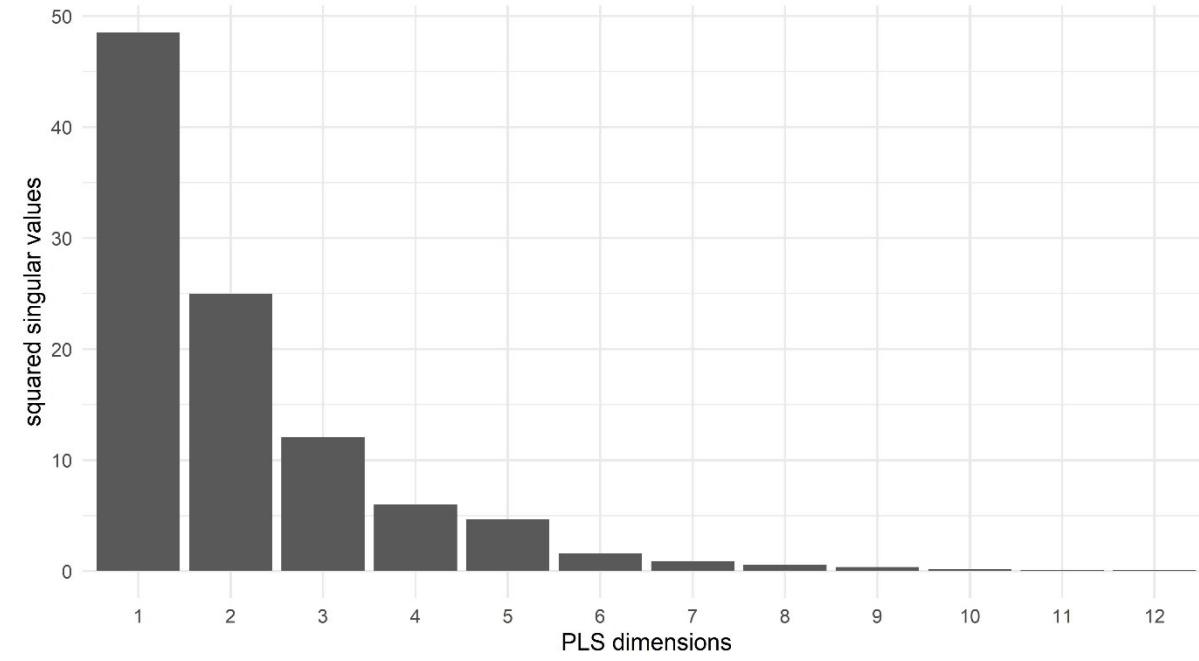

Figure 23: scree plot displaying the percentage of the total squared covariance for the first twelve PLS components

The fraction of squared covariance for the partial least squares dimensions (Figure 23) begins to drop off on the third component. It will still be considered along components one and two.

The first singular vector of the PLS (Figure 24) captures the difference between aquatic species on the far-left side of the scatterplot and the rest. All characteristics that do not apply to an aquatic lifestyle, such as terrestrial, scansorial, fossorial lifestyles and orthogrady vs pronogrady, face in the opposite direction. The aquatic species are all placed on the left side of the scatterplot.

Figure 25 visualizes the specimens' scores for partial least squares dimension one. Specimens with a high ecological score in PLS dimension one (Figure 26) are characterized by a relatively short and wide cochlea with a narrower second turn. Specimen with a low value for the ecological score (Figure 27) have a more strongly tapering cochlea that is generally less wide. The vestibule is bigger, and the semicircular canals extend more in the superior – inferior direction.
The shape component of PLS dimension one is characterized by a predicted shape with a very short cochlea base on the top (Figure 28). The semicircular canals are enlarged

relatively to the rest of the shape. The vestibule takes up very little space. Specimens with a low ecological score (Figure 29) have small semicircular canals and a large vestibule. The base of the cochlea is elongated, the cochlea itself is wide and flat.

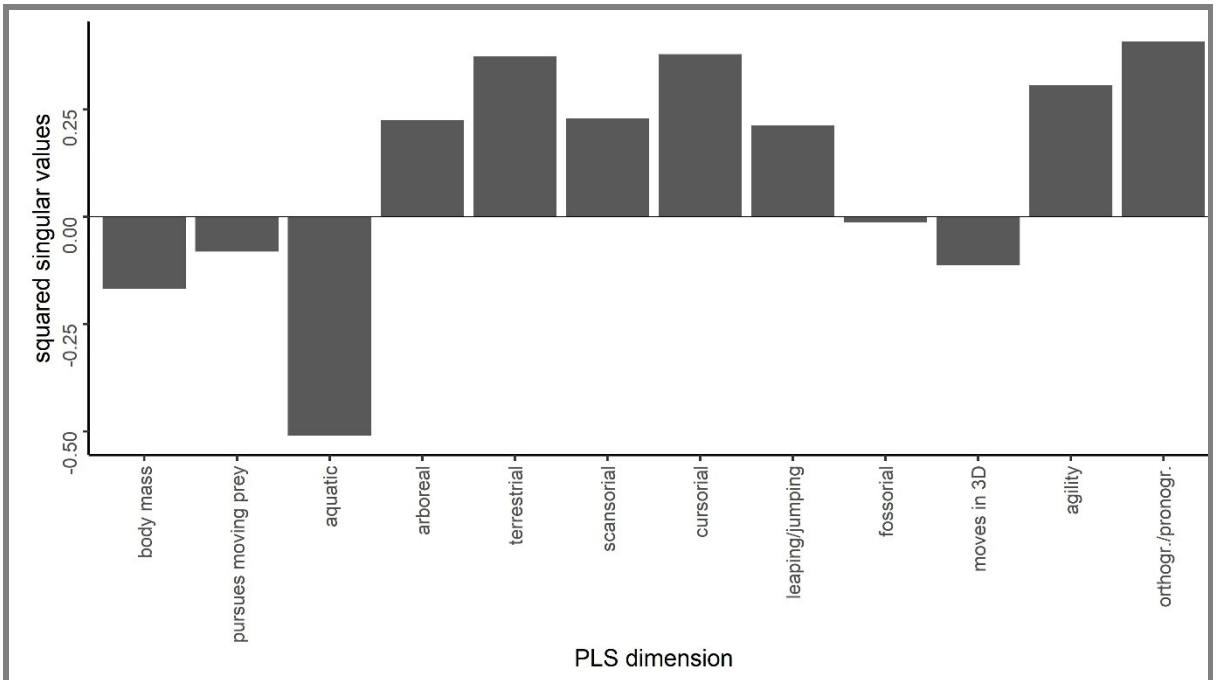

Figure 24: bar plot displaying the first singular vector of the PLS result

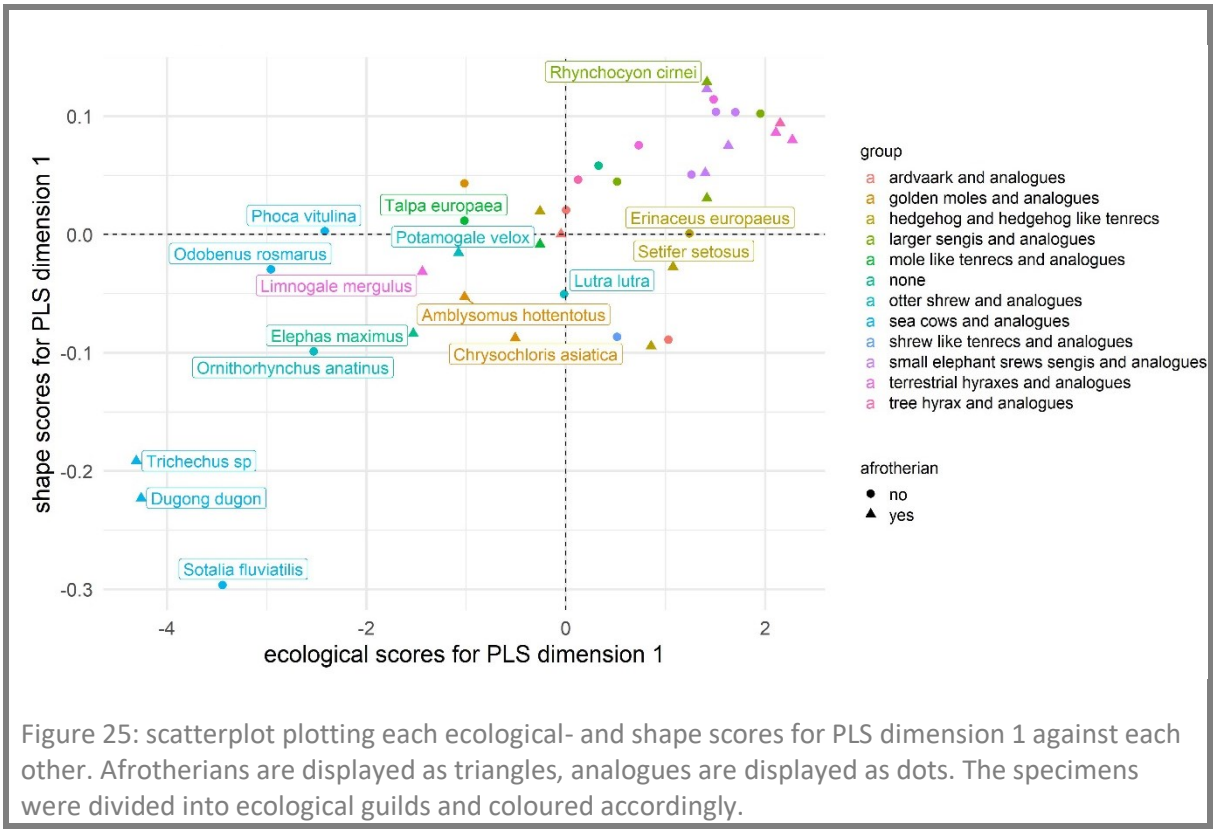

Figure 25: scatterplot plotting each ecological- and shape scores for PLS dimension 1 against each other. Afrotherians are displayed as triangles, analogues are displayed as dots. The specimens were divided into ecological guilds and coloured accordingly.

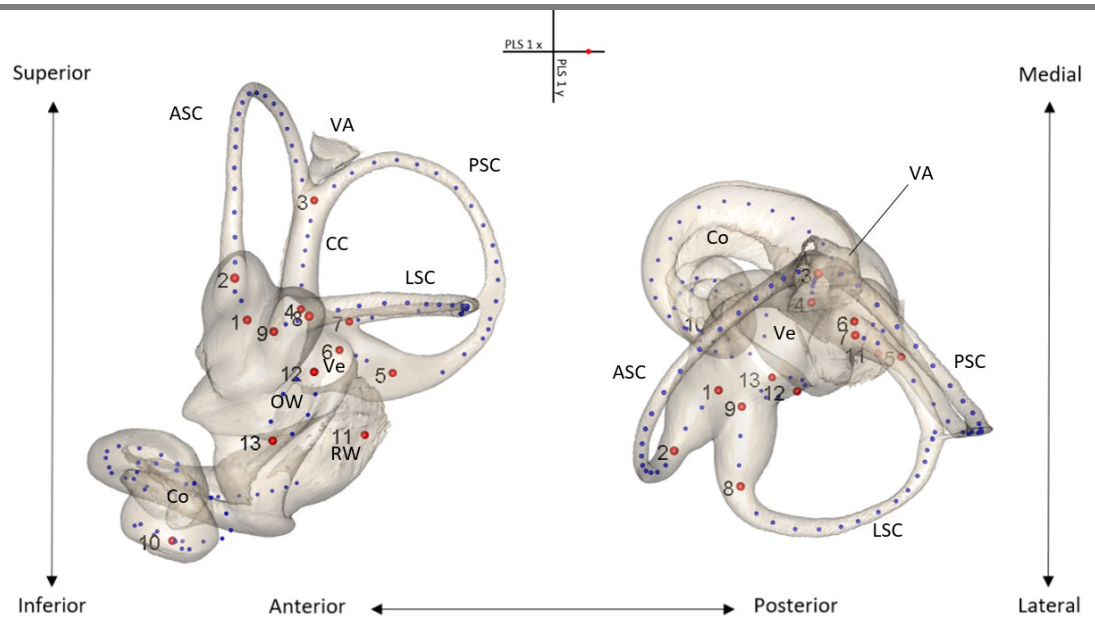

Figure 26: Predicted shape configuration of a specimen with a high ecological score (PLS 1 x) for the and an average shape score (PLS 1 y) in PLS dimension 1 both lateral (left) and superior (right) view. Landmarks are displayed in red and are numbered, semilandmarks are displayed in blue. *ASC*, anterior semicircular canal; *PSC*, posterior semicircular canal; *LSC*, lateral semicircular canal; *CC*, common crus; *VA*, vestibular aqueduct; *Ve*, vestibule; *OW*, oval window; *RW*, round window; *Co*, cochlea

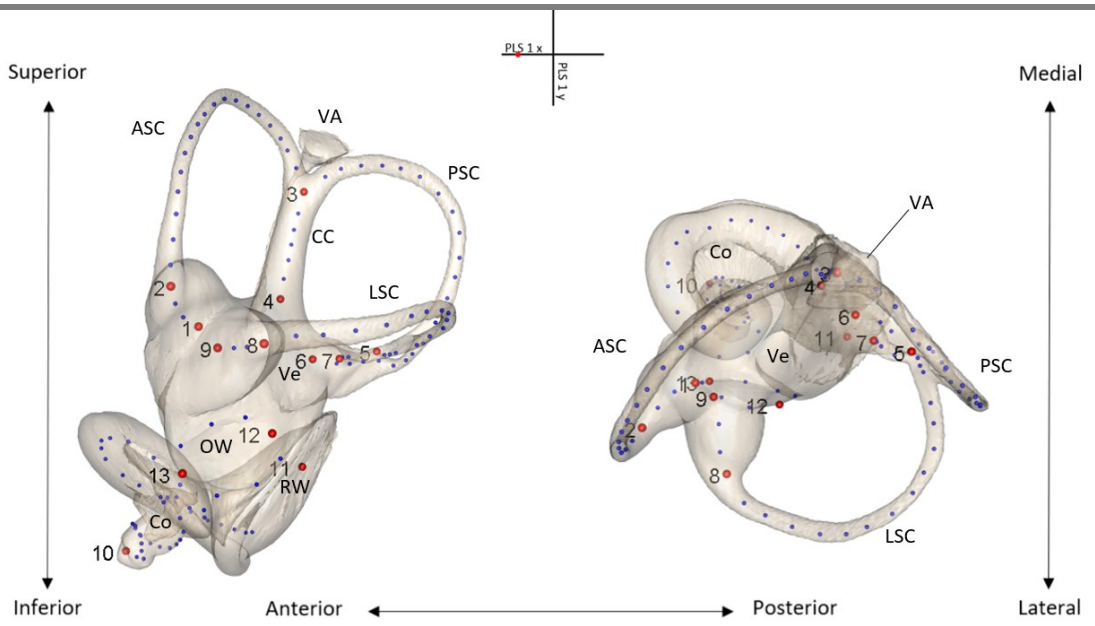

Figure 27: Predicted shape configuration of a specimen with a low ecological score (PLS 1 x) for the and an average shape score (PLS 1 y) in PLS dimension 1 both lateral (left) and superior (right) view. Landmarks are displayed in red and are numbered, semilandmarks are displayed in blue. *ASC*, anterior semicircular canal; *PSC*, posterior semicircular canal; *LSC*, lateral semicircular canal; *CC*, common crus; *VA*, vestibular aqueduct; *Ve*, vestibule; *OW*, oval window; *RW*, round window; *Co*, cochlea.

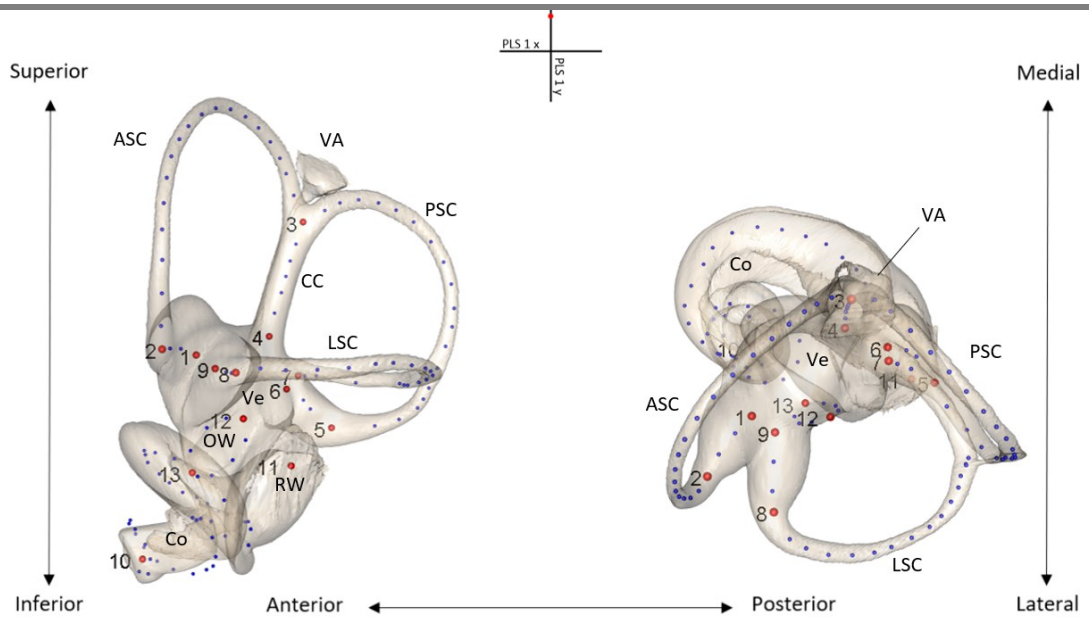

Figure 28: Predicted shape configuration of a specimen with an average ecological score (PLS 1 x) for the and a high shape score (PLS 1 y) in PLS dimension 1 both lateral (left) and superior (right) view. Landmarks are displayed in red and are numbered, semilandmarks are displayed in blue. *ASC*, anterior semicircular canal; *PSC*, posterior semicircular canal; *LSC*, lateral semicircular canal; *CC*, common crus; *VA*, vestibular aqueduct; *Ve*, vestibule; *OW*, oval window; *RW*, round window; *Co*, cochlea.

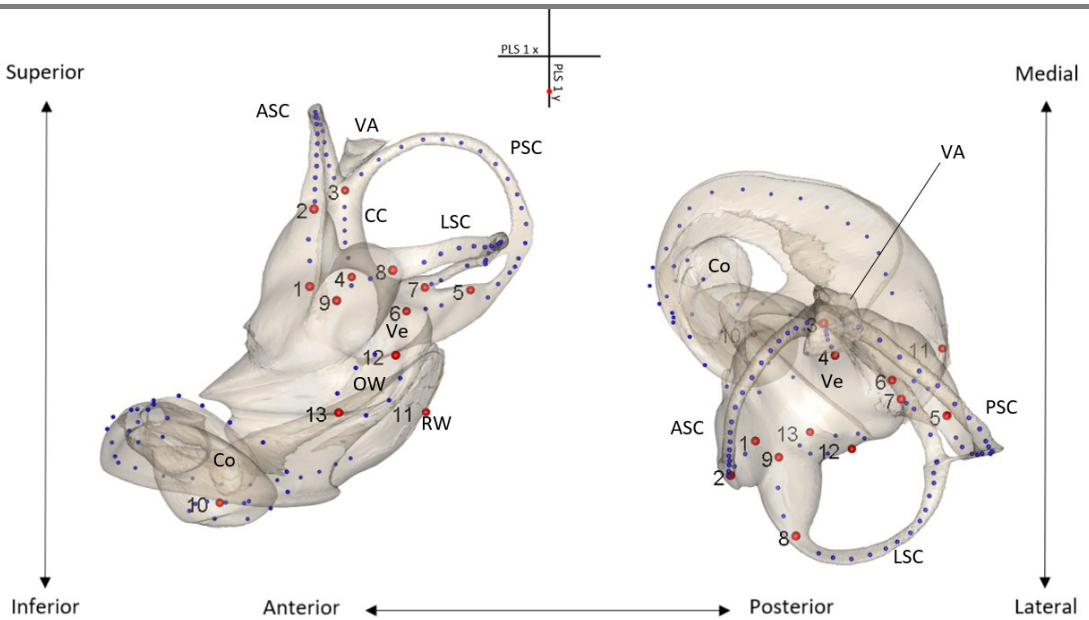

Figure 29: Predicted shape configuration of a specimen with a low ecological score (PLS 1 x) for the and an average shape score (PLS 1 y) in PLS dimension 1 both lateral (left) and superior (right) view. Landmarks are displayed in red and are numbered, semilandmarks are displayed in blue. *ASC*, anterior semicircular canal; *PSC*, posterior semicircular canal; *LSC*, lateral semicircular canal; *CC*, common crus; *VA*, vestibular aqueduct; *Ve*, vestibule; *OW*, oval window; *RW*, round window; *Co*, cochlea.

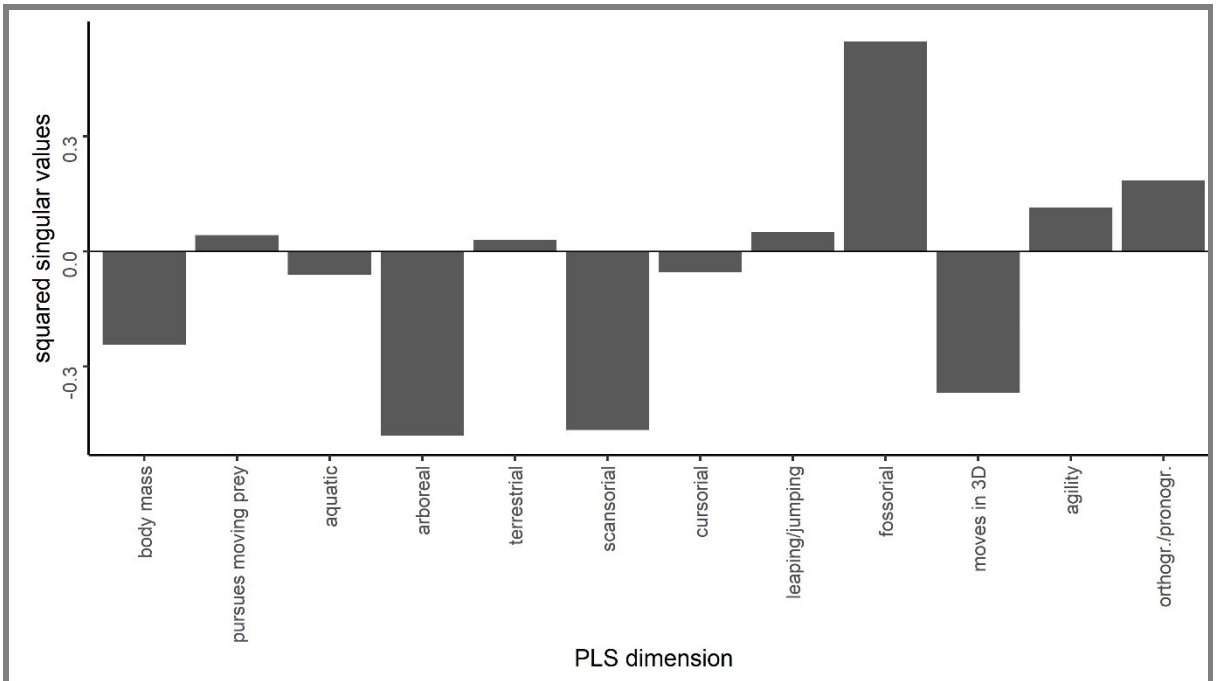

Figure 30: bar plot displaying the second singular vector of the PLS result

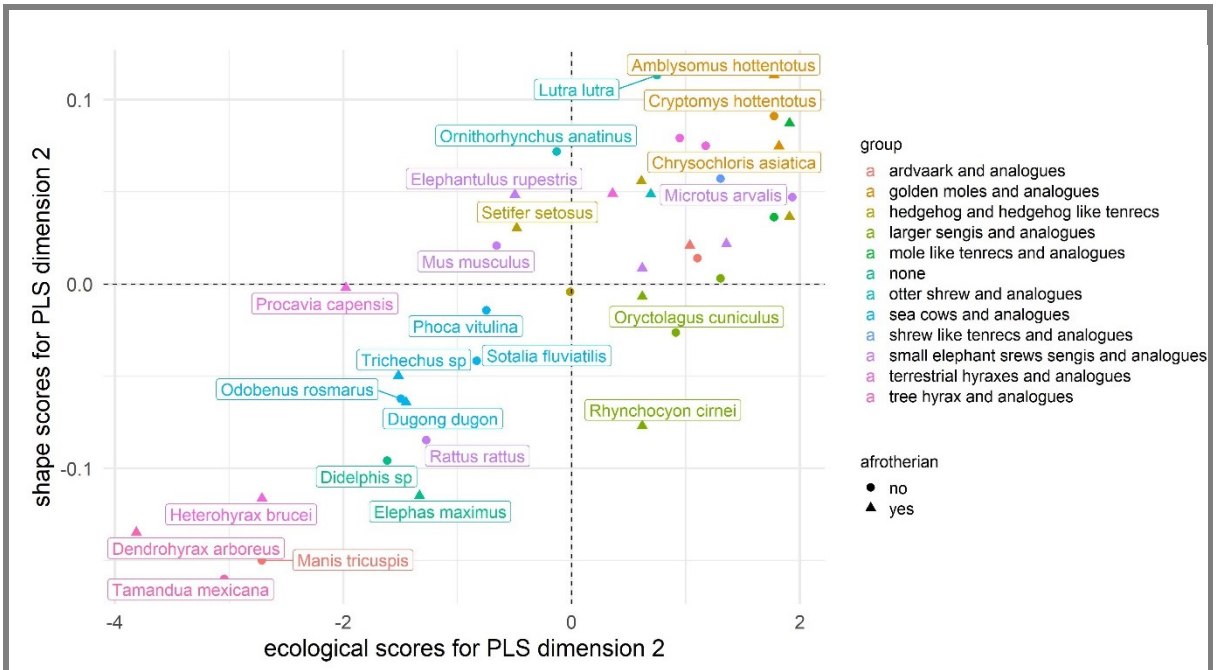

Figure 31: Scatterplot plotting each ecological- and shape scores for PLS dimension 2 against each other. Afrotherians are displayed as triangles, analogues are displayed as dots. The specimens were divided into ecological guilds and coloured accordingly.

Figure 30 visualizes the specimens scores for partial least squares dimension two.
Specimens with a high ecological score in PLS dimension two (Figure32) are characterized by a strongly coiled cochlea with a widened base.
Specimen with a low value for the ecological score (Figure33) have a strongly coiled cochlea with a narrow base.

The shape component of PLS dimension two is characterized by a flat and wide cochlea on the top (Figure 34). Specimens with low ecological score (Figure 35) have a large cochlea with a wide base.

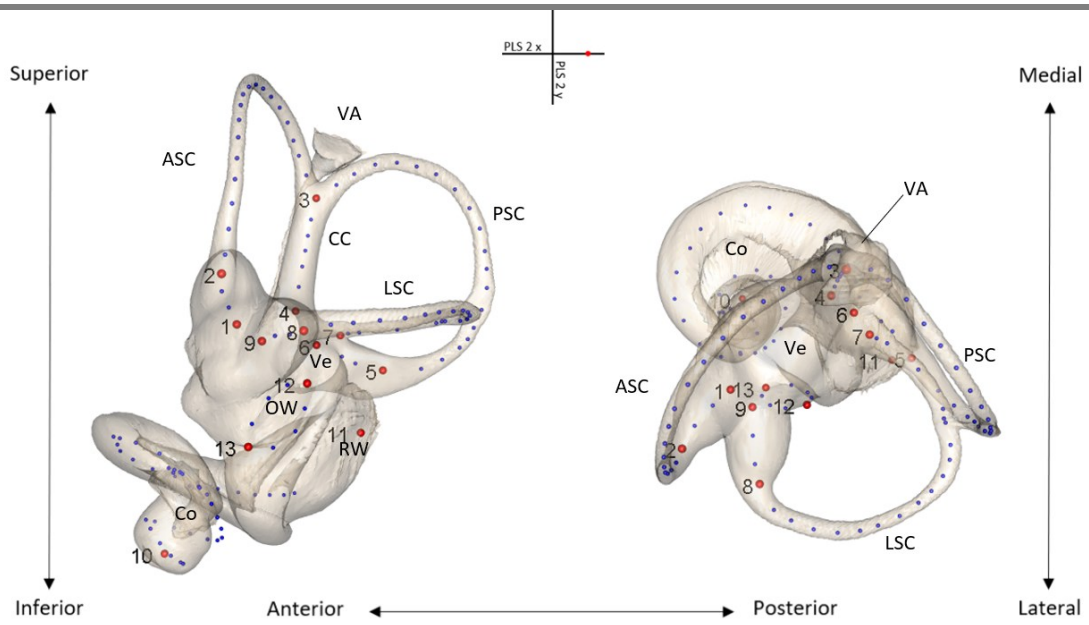

Figure 32: Predicted shape configuration of a specimen with a high ecological score (PLS 2 x) for the and an average shape score (PLS y y) in PLS dimension 2 both lateral (left) and superior (right) view. Landmarks are displayed in red and are numbered, semilandmarks are displayed in blue. *ASC*, anterior semicircular canal; *PSC*, posterior semicircular canal; *LSC*, lateral semicircular canal; *CC*, common crus; *VA*, vestibular aqueduct; *Ve*, vestibule; *OW*, oval window; *RW*, round window; *Co*, cochlea.

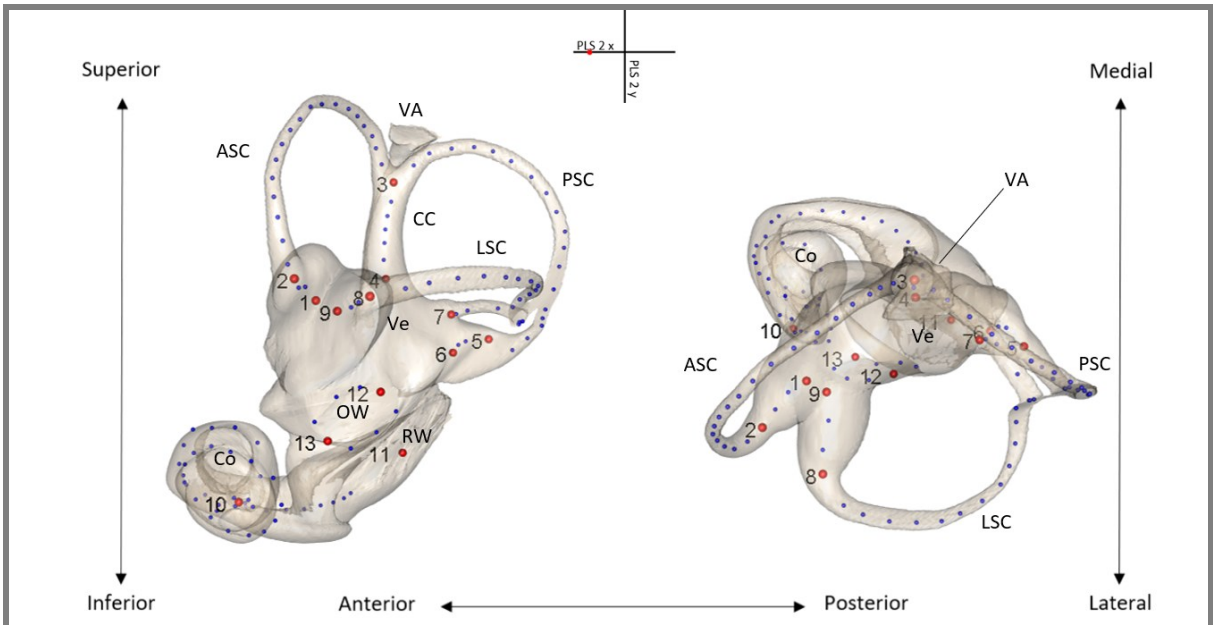

Figure 33: Predicted shape configuration of a specimen with a low ecological score (PLS 2 x) for the and an average shape score (PLS y y) in PLS dimension 2 both lateral (left) and superior (right) view. Landmarks are displayed in red and are numbered, semilandmarks are displayed in blue. *ASC*, anterior semicircular canal; *PSC*, posterior semicircular canal; *LSC*, lateral semicircular canal; *CC*, common crus; *VA*, vestibular aqueduct; *Ve*, vestibule; *OW*, oval window; *RW*, round window; *Co*, cochlea.

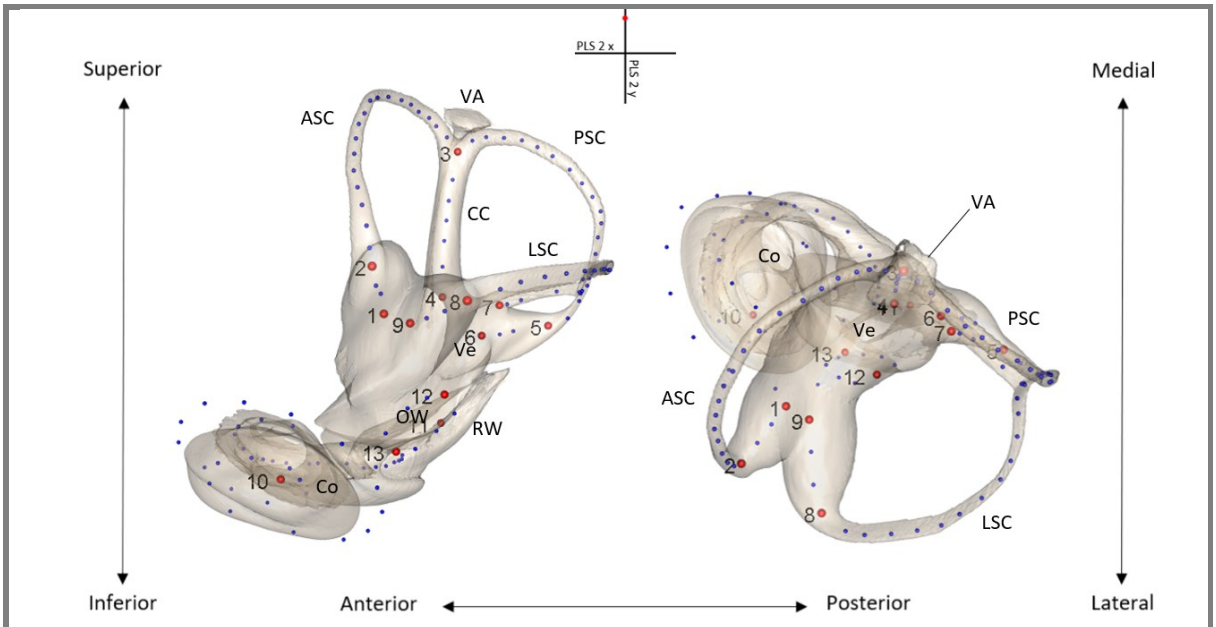

Figure 34: Predicted shape of a specimen with an average ecological score (PLS 2 x) for the and a high shape score (PLS y y) in PLS dimension 2 both lateral (left) and superior (right) view. Landmarks are displayed in red and are numbered, semilandmarks are displayed in blue. *ASC*, anterior semicircular canal; *PSC*, posterior semicircular canal; *LSC*, lateral semicircular canal; *CC*, common crus; *VA*, vestibular aqueduct; *Ve*, vestibule; *OW*, oval window; *RW*, round window; *Co*, cochlea.

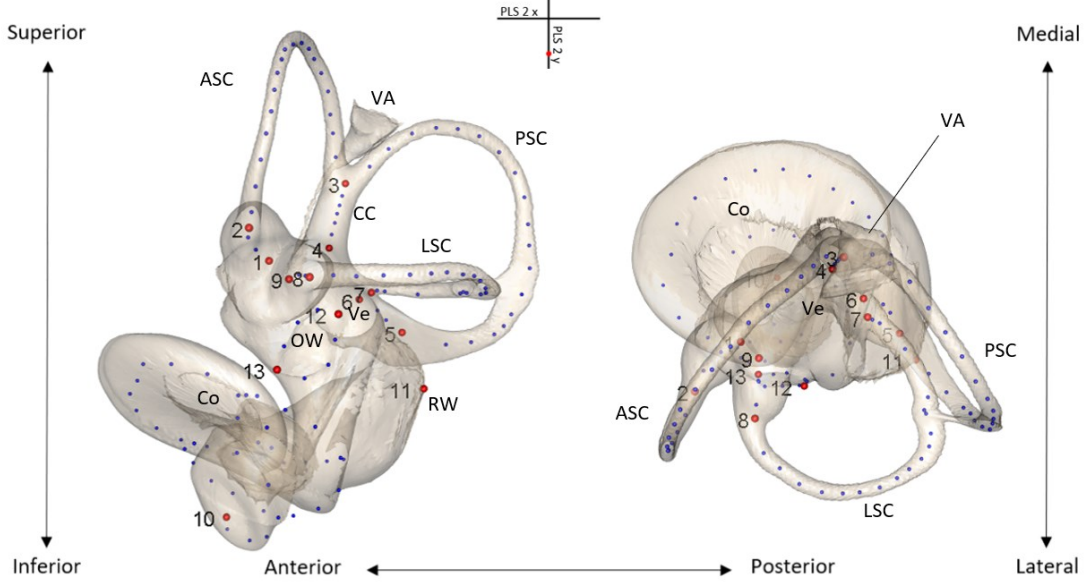

Figure 35: Predicted shape configuration of a specimen with an average ecological score (PLS 2 x) for the and a low shape score (PLS y y) in PLS dimension 2 both lateral (left) and superior (right) view. Landmarks are displayed in red and are numbered, semilandmarks are displayed in blue. *ASC*, anterior semicircular canal; *PSC*, posterior semicircular canal; *LSC*, lateral semicircular canal; *CC*, common crus; *VA*, vestibular aqueduct; *Ve*, vestibule; *OW*, oval window; *RW*, round window; *Co*, cochlea.

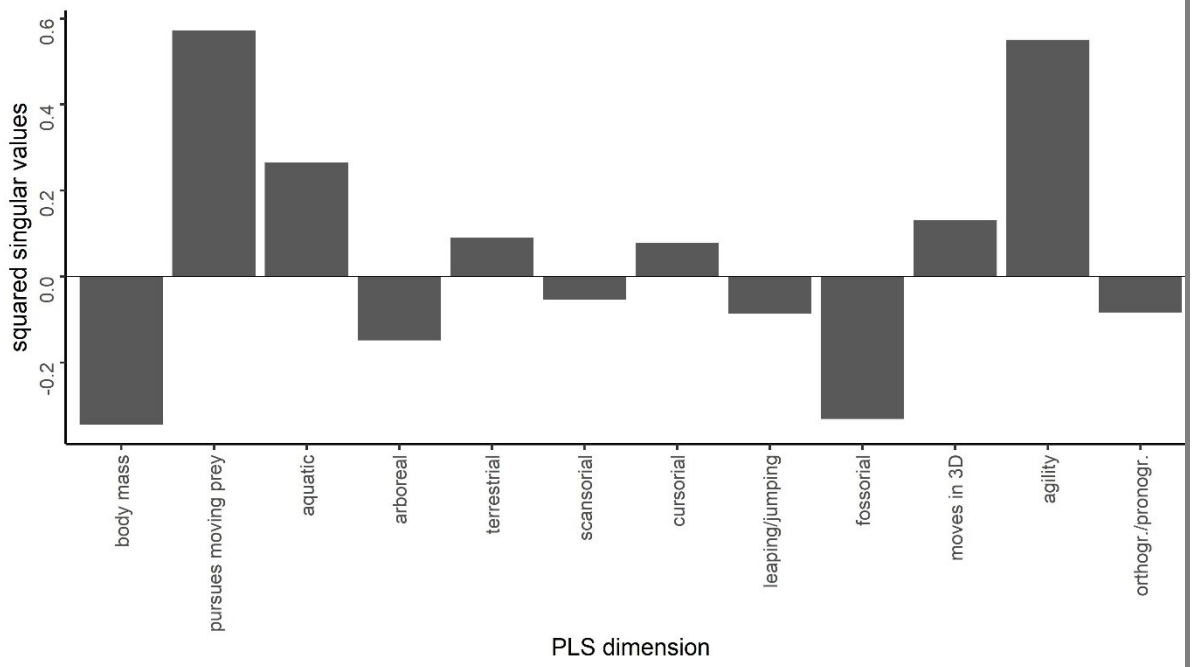

Figure 36: barplot displaying the third singular vector of the PLS result

Agility and the pursuit of moving prey point in the same direction, which is clearly biologically meaningful. This is contrasted with body mass. It is interesting that those components were not relevant before.

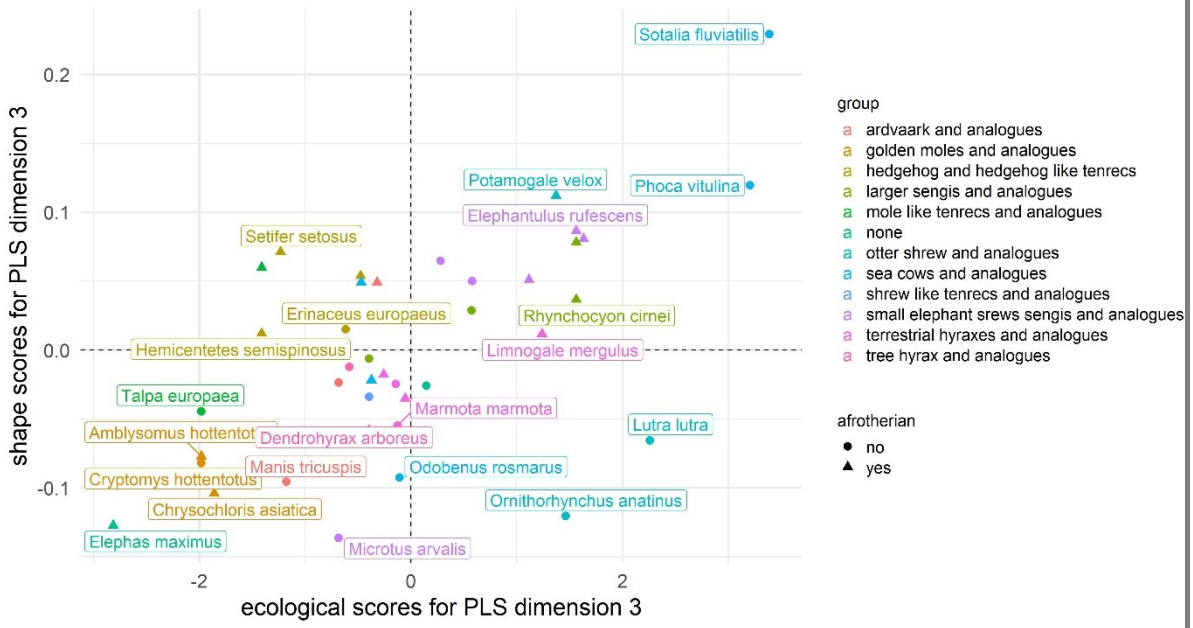

Figure 37: scatterplot plotting each ecological- and shape scores for PLS dimension 3 against each other. Afrotherians are displayed as triangles, analogues are displayed as dots. The specimens were divided into ecological guilds and coloured accordingly.

Figure 36 visualizes the specimens scores for partial least squares dimension three.
Specimens with a high ecological score in PLS dimension three (Figure 38) are characterized by a relatively small, strongly coiled cochlea with a taper in the inferior direction and a base that is particularly close to the vestibule. The semicircular canals are relatively large, especially the anterior semicircular canal.
Specimens with a low value for the ecological score in PLS dimension three (Figure39) have smaller semicircular canals.
The shape component of PLS dimension three is characterized by a very wide and large cochlea on the top (Figure40). The first turn of the cochlea sits again very close to the vestibule. The semicircular canals are small. Specimens with low ecological score (Figure41) have a small, strongly coiled cochlea with a shortened base.

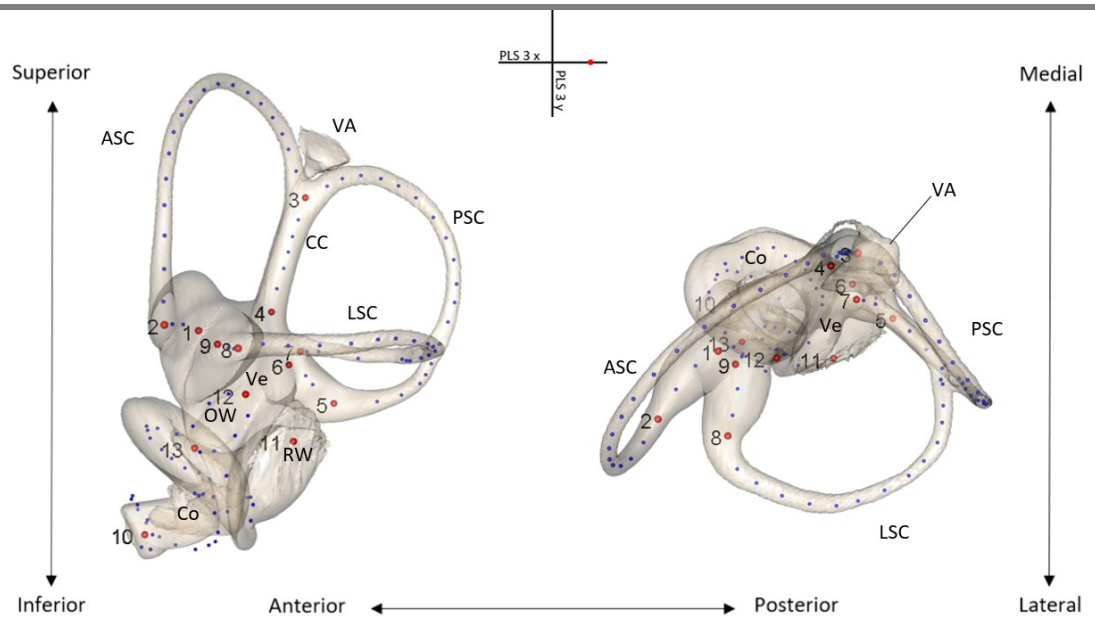

Figure 38: Predicted shape configuration of a specimen with a high ecological score (PLS 3 x) for the and an average shape score (PLS 3 y) in PLS dimension 3 both lateral (left) and superior (right) view. Landmarks are displayed in red and are numbered, semilandmarks are displayed in blue. *ASC*, anterior semicircular canal; *PSC*, posterior semicircular canal; *LSC*, lateral semicircular canal; *CC*, common crus; *VA*, vestibular aqueduct; *Ve*, vestibule; *OW*, oval window; *RW*, round window; *Co*, cochlea.

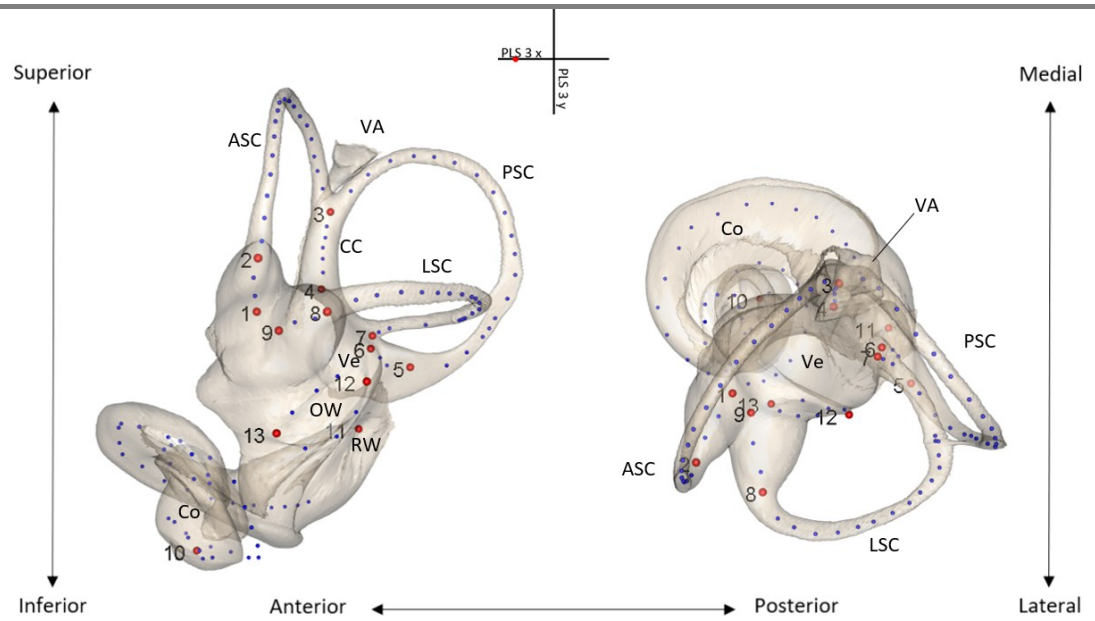

Figure 39: Predicted shape configuration of a specimen with a low ecological score (PLS 3 x) for the and an average shape score (PLS 3 y) in PLS dimension 3 both lateral (left) and superior (right) view. Landmarks are displayed in red and are numbered, semilandmarks are displayed in blue. *ASC*, anterior semicircular canal; *PSC*, posterior semicircular canal; *LSC*, lateral semicircular canal; *CC*, common crus; *VA*, vestibular aqueduct; *Ve*, vestibule; *OW*, oval window; *RW*, round window; *Co*, cochlea.

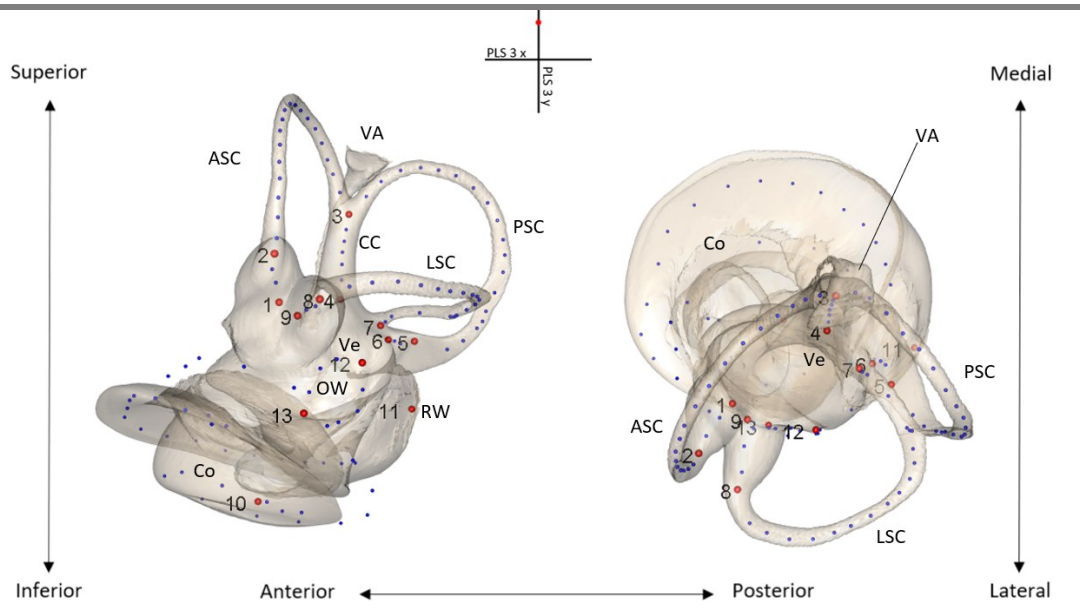

Figure 40: Predicted shape configuration of a specimen with an average ecological score (PLS 3 x) for the and a high shape score (PLS 3 y) in PLS dimension 3 both lateral (left) and superior (right) view. Landmarks are displayed in red and are numbered, semilandmarks are displayed in blue. *ASC*, anterior semicircular canal; *PSC*, posterior semicircular canal; *LSC*, lateral semicircular canal; *CC*, common crus; *VA*, vestibular aqueduct; *Ve*, vestibule; *OW*, oval window; *RW*, round window; *Co*, cochlea.

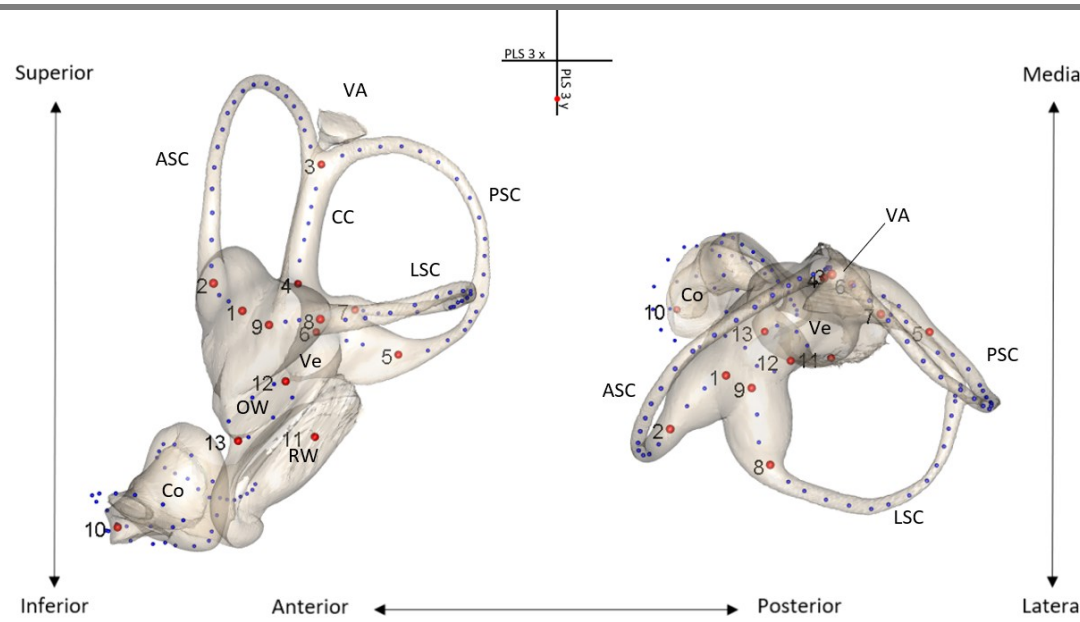

Figure 41: Predicted shape configuration of a specimen with an average ecological score (PLS 3 x) for the and a low shape score (PLS 3 y) in PLS dimension 3 both lateral (left) and superior (right) view. Landmarks are displayed in red and are numbered, semilandmarks are displayed in blue. *ASC*, anterior semicircular canal; *PSC*, posterior semicircular canal; *LSC*, lateral semicircular canal; *CC*, common crus; *VA*, vestibular aqueduct; *Ve*, vestibule; *OW*, oval window; *RW*, round window; *Co*, cochlea.

Discussion

Obligatory Aquatic Lifestyle

The difference between obligatory aquatic species, which include *Sotalia* fluvitalis, *Trichechus sp.*, and *Dugong dugon*, from the rest of the sample clearly dominated PLS dimension 1 (Figure 24 and 25). Despite some overlap, the first two principal components (Figure6) also seem to capture this difference.
Sotalia fluvitalis is the most prominent representant of this group. It has an especially large cochlea and relatively small semicircular canals which is captured by principal component one (Figure7). Those features are shared to a lower extent by *Trichechus sp.* and *Dugong dugon*, those two specimens also have an enlarged vestibule which is captured in PC 1 (Figure8). The lower degree of cochlea coiling, and large cochlea present in these three species is likely what is captured in principal component two (Figure9). These features stretch across phylogenetically distant groups.
According to Köppl and Manley (2019), an increase in cochlea length can come both with an increase in frequency range (in both directions), because octaves occupy roughly similar spaces. More space per octave could on the other hand be used to increase frequency selectivity (Köppl and Manley, 2019). The audiogram in figure 42 highlights the Tucuxi (*Sotalia fluvitalis*) ability to detect sounds at very high frequencies up to 135 kHz. Such relatively high-frequency echolocation abilities are required by delphinids living in habitats such as estuaries or rivers in order to differentiate objects in such structurally complex environments (Sauerland and Dehnhardt, 1998). While high frequency hearing is not as well developed in sea cows (*Trichechus sp.*), their hearing capabilities still extend far into the ultrasonic range, making them able to detect sound cues at a maximum frequency of at least 45 kHz (Gerstein et al., 1999). Marine mammals in general have peak hearing capacities at ultrasonic frequencies as an evolutionary response to the auditory physics of the marine environment (Wartzok and Ketten, 1999). Shape adaptations to high frequency hearing might therefore serve as an explanation for the unproportionally big cochlea in the obligatory aquatic species.

Subterranean lifestyle

Hearing in subterranean mammals tends to be restricted to lower frequencies (Brückman and Burda, 1997). Figure43 features an audiogram of *Cryptomys sp.*, showing sensitivity to low-frequency sounds. This is likely due to higher frequencies being filtered out in subterranean tunnels (Burda et al., 1992), where the least attenuation of sound occurs at around 500 Hz (Brückman and Burda, 1997). Subterranean mammals have low hearing sensitivity and are not well equipped to localize airborne sound (Brückman and Burda, 1997). This is likely due to higher frequencies being filtered out and losing their biological significance (Burda et al., 1992). There has been a debate whether hearing in subterranean mammals is vestigial or adaptive, finding some features of their auditory organs to be vestigial, while also finding signs for adaptation, consisting of convergent occurrences of similar features reported by several morphologists (Brückman and Burda, 1997). Morphometric studies on shape adaptations of the cochlea to low frequency hearing has been conducted by West (1985), who found the product of the number of cochlea turns with basilar membrane length to correlate strongly with low frequency hearing limits.

In a later study Manoussaki et al. (2008) built on the theory that the cochlea's graded curvature enhances the mechanical response to low frequency hearing. They found the ratio of the radii of curvature from the outermost and innermost turns of the cochlear correlating strongly with low-frequency hearing limits. Therefore, we would expect the subterranean cochlea to have multiple turns and taper strongly in the anterior/inferior direction. The shape prediction for a low score in principal component 6 (Figure20) shows those features to a strong degree, it also corresponds to the position of the *Cryptomys hottentotus* in the scatterplot (Figure16). PLS dimension 2 reflects this in the ecological component (Figure34). PLS 3 also captures this partly (Figure41, Figure39, and Figure37).

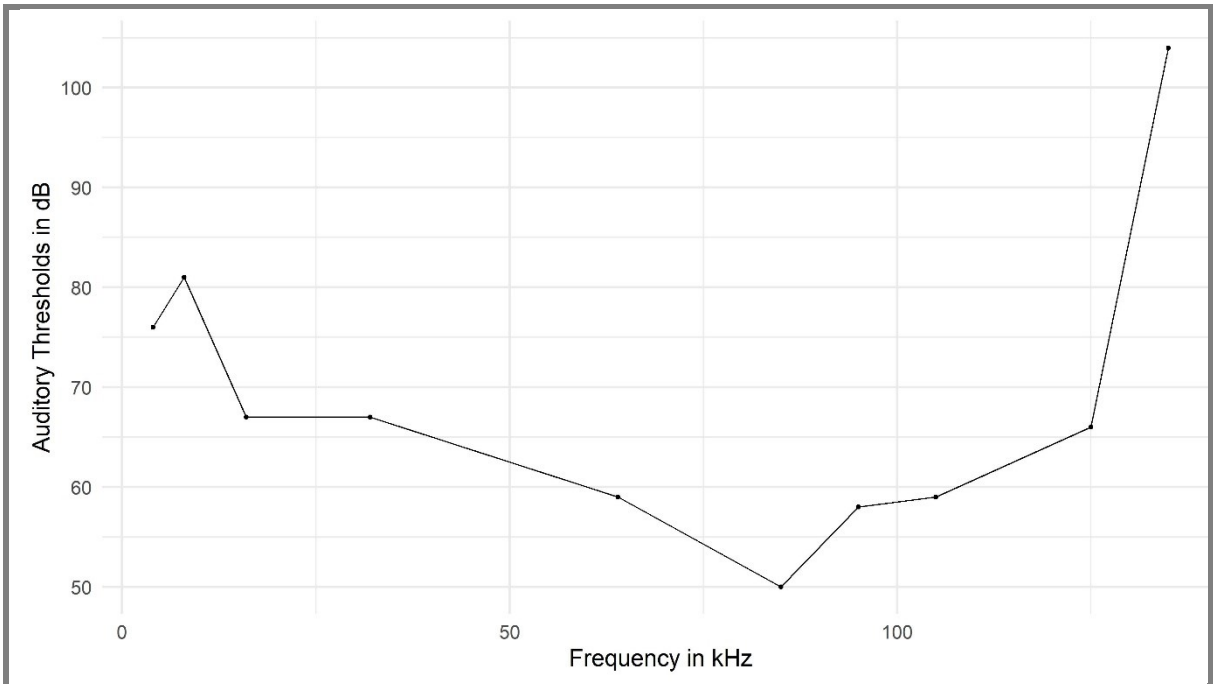

Figure42: underwater audiogram of *Sotalia fluvitalis*, taken from Sauerland and Derhardt (1998)

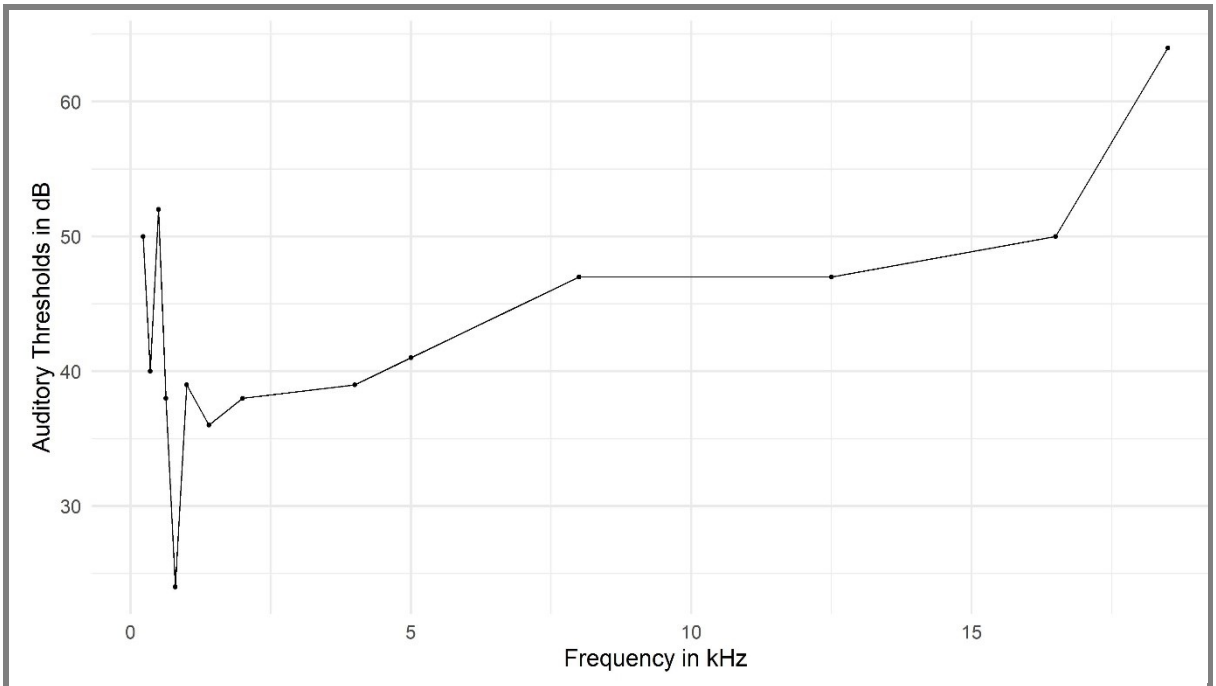

Figure43: audiogram of *Cryptomys. sp*., taken from Brückman and Burda (1997)

Afrotherian Features

No distinctly afrotherian inner ear shape or shape component could be determined. From visual inspection of inner ear shapes, I hypothesized about increased cochlea coiling or a secondary common cruz, which is a partly fused lateral and posterior secondary semicircular canal, being more prevalent in afrotheria. The occurrence of those features among mammals has been studied to some extent (see for example Ekdale, 2013 and Benoit et al., 2015). The secondary common cruz seems to be basal feature, its absence is derived for placental mammals (Ekdale, 2015). It is present in some afrotherians, for example in *Orycteropus afer*, but can also be found in other placental mammals such as wolves (*Canis sp.*) (Ekdale, 2015) and marsurpials such as *Didelphis sp*. Intense cochlea coiling can be observed in some afrotherians, such as *Cryptomys sp.* but is also present to an even greater extant in other placental mammals, notably Guina Pigs (*Cavia sp.*) (Ekdale, 2015). Aquatic afrotherians such as *Trichechus manatus* have an especially low degree of cochlea coiling.

Evolution of the Middle Ear

As was already mentioned in the introduction, the evolution of the secondary jaw joint was a crucial prerequisite for the evolution of the mammalian middle ear (Fish, 2019). The quadrate, articular and angular bones of early synapsids are homologous to the incus, malleus, gonial and ectotympanic bones of derived mammals (Navarro-Díaz et al., 2019). A middle ear transmitting vibrations from air to the fluids of the inner ear is an important adaptation to terrestrial life, which is highlighted by it evolving in multiple lineages (Fish, 2019). The mammalian jaw joint likely evolved in multiple stages, starting with a rearrangement of muscles for mastication in response to changes in dentition (Anthwal and Tucker, 2022). This caused an alteration of the arrangement of the jaw closure musculature, which also allowed for a wider range of jaw movement (Anthwal and Tucker, 2022). All of these changes enabled mammals to exploit a growing number of herbivore niches coming about by the angiosperm radiation (Anthwal and Tucker, 2022). After the evolution of the secondary jaw joint, the ancestral jaw joint was free to evolve into a sound transmission structure (Navarro-Díaz et al., 2019). In recent years the rich fossil record and developmental studies allowed for the reconstruction of the evolution of the middle ear ossicles (Navarro-Díaz et al., 2019). The post dentary bones evolved to improve sound transmission from the lower jaw to the inner ear, their reduction in size and disconnection from the cranium increased the bones vibrational mobility, thereby improving sound sensitivity (Navarro-Díaz et al., 2019). This whole development is in accordance with Willistons Law, which says that evolution often reduces the number of cranial elements with the remaining ones becoming more specialized (Navarro-Díaz et al., 2019).

Evolvability of the Inner Ear

The various scatterplots from the PCA and PLS (Figure6, 11, 16, 25, 31, 37) exhibit little to no clustering of afrotherians against the analogue species. The PLS was able to filter out meaningful connections based only on inner ear shape and ecological variables. It is therefore observable that similar ecological adaptations were made in phylogenetically distant groups, overcoming phylogenetic constraints. This goes against the theoretical

limitations to inner ear evolvability mentioned in the introduction. Possible explanations for this are numerous.
According to Kirschner and Gerhart (1998), evolvability, in the sense of a capacity to generate heritable, selectable phenotypic variation, has two main components: first, a reduction of potential lethality of mutations and second, a reduction in the number of mutations needed to produce phenotypically novel traits. I want to extend the first point by a reduction in not only lethality but all kinds of fitness loss due to new mutations for the purpose of this discussion. Among others, Kirschner and Gerhart (1998) mentioned compartmentation as an important and widely recognized stratagem of evolvability. Sub-division of not only structures in the phenotype but also of the developmental and regulatory processes that create them, removes interdependencies, thereby reducing the risk of changes in one structure inhibiting the formation and function of other organismal parts. This constitutes a reduction in possible fitness loss due to new mutations. Riedl (1978) therefore predicted in his imitatory epigenotype hypothesis, that the pattern of developmental constraints would reflect the pattern of functional constraints. In contemporary literature the term modularity is used instead (Wagner and Altenberg, 1996; Mitteroecker et al, 2012).
On the other hand modularity is not the only potential property of the genotype phenotype map that can achieve evolvability (Hansen, 2003). Pavlicev and Hansen (2011) used a deterministic model to show, that the highest possible evolvability is achieved through maximization of genetic variance and minimization of genetic covariance, which can be achieved through modularity, but also through patterns of pleiotropy that cancel each other out. This has also been shown by Mitteroecker (2009).
In light of the evolutionary history of the mammalian ear region, the concepts mentioned above lend themselves well to explain the high evolvability of the region observed here. During the transition from non-mammalian synapsids to crown mammals the individual bones of the jaw gradually reduced into a single element, while the jaw bones got incorporated into the middle ear complex (Lautenschlager et al., 2017). According to Le Maître et al. (2020) this transition, which most likely initially benefited mastication and was therefore under positive selection (Lautenschlager et al., 2017), increased the genetic, regulatory, and developmental complexity of the mammalian ear. This increased the evolvability of the ear because it decoupled hearing from masticatory functions (Mao et al., 2019) as well as increase the evolutionary degrees of freedom, by adding more developmentally independent components that could be adapted to different functional units independently (Le Maître et al., 2020).

Conclusion

This work contributed to demonstrating that inner ear shape is more influenced by environmental than phylogenetic constraints, by comparing shape variation in afrotherian species to shape variation in more distantly related, yet ecologically similar analogue species. It also raised the question on how the mammalian inner ear, as one of their key senses could be adapted to function in a wide range of ecological regimes and be the site of evolutionary novelties despite being theoretically constrained with respect to its evolvability.
More research is needed to give a satisfactory answer to this question. Increasing the sample size per species while retaining the overall methodology employed in this work would allow for the comparison of intraspecific to interspecific variation. This would in turn enable the use of measurements for evolvability developed by Hansen and Houle (2008),

enabling researchers to quantify evolution and constraint on shape features of the mammalian inner ear. Similar research could also be extended to include the middle ear ossicles, as they were strongly affected by the mammalian jaw transformation and key to mammalian high frequency hearing capabilities. Comparisons between mammalian inner and middle ears to those of other groups such as birds might also contribute to uncovering unique evolutionary properties of the mammalian ear.

Understanding how unique mammalian ear features developed by reconstructing and investigating shapes of fossilized mammals could also be a contribution to an understanding of the evolvability of the mammalian ear.

Developmental research into the ear could uncover the pleiotropic structure of the region, which would lead to a better understanding of developmental constraints and how they affect evolvability.

Literature

Adams, D. C., Collyer, M. L., Kaliontzopoulou, A., and Baken, E.K. (2022). Geomorph: Software for geometric morphometric analyses. R package version 4.0.4. https://cran.r-project.org/package=geomorph

Anthwal, N., Tucker, A. S., (2022). Evolution and development of the mammalian jaw joint: Making a novel structure. Evolution & Development. 2023;25:3–14. doi: 10.1111/ede.12426

Baken, E. K., Collyer, M. L., Kaliontzopoulou, A., and Adams, D. C. (2021). geomorph v4.0 and gmShiny: enhanced analytics and a new graphical interface for a comprehensive morphometric experience. Methods in Ecology and Evolution. 12:2355-2363.

Benoit, J., Lehmann, T., Vatter, M., Lebrun, R., Merigeaud, S., Costeur, L., Tabuce, R. (2015). Comparative Anatomy and Three-Dimensional Geometric-Morphometric Study of the Bony Labyrinth of Bibymalagasia (Mammalia, Afrotheria). Journal of Vertebrate Paleontology e930043. doi: 10.1080/02724634.2014.930043

Boosktein, F.L. (1996). Biometrics, Biomathematics and the Morphometric Synthesis. Bulletin of Mathematical Biology, Vol. 58, No. 2, pp. 313-365

Bougeard S., Dray S. (2018). Supervised Multiblock Analysis in R with the ade4 Package. _Journal of Statistical Software_, *86*(1), 1-17. doi: 10.18637/jss.v086.i01 (URL: https://doi.org/10.18637/jss.v086.i01).

Brückmann, G., Burda H. (1997). Hearing in blind subterranean Zambian mole-rats (Cryptomys sp.): collective behavioural audiogram in a highly social rodent. J Comp Physiol A (1997) 181: 83±88

Burda, H., Bruns, V., Hickman, G. C. (1992). The Ear in Subterranean lnsectivora and Rodentia in Comparison With Ground-Dwelling Representatives. I. Sound Conducting System of the Middle Ear. Journal Of Morphology 214:49-61

Burda, H., Bruns, V., Hickman, G.C. (1992). The Ear in Subterranean lnsectivora and Rodentia in Comparison With Ground-Dwelling Representatives. I. Sound Conducting System of the Middle Ear. JOURNAL OF MORPHOLOGY 214:49-61 (1992)

Chessel, D., Dufour, A., Thioulouse, J. (2004). The ade4 Package - I: One-Table Methods. _R News_, *4*(1), 5-10. <URL: https://cran.r-project.org/doc/Rnews/>.

Cox, P. G., and Jeffery, N. (2010). Semicircular canals and agility: the influence of size and shape measures. J. Anat. 216, pp37–47. doi: 10.1111/j.1469-7580.2009.01172.x

de Jong, W. W., Zweers, A., Goodman, M. (1981). Relationship of ardvaark to elephant, hyraxes and sea cows from α-crystallin sequences. Nature 292:538–540.

Dray, S., Dufour, A. (2007). The ade4 Package: Implementing the Duality Diagram for Ecologists. _Journal of Statistical Software_, *22*(4), 1-20. doi: 10.18637/jss.v022.i04 (URL: https://doi.org/10.18637/jss.v022.i04).

Dray, S., Dufour ,A., Chessel D. (2007). The ade4 Package - II: Two-Table and K-Table Methods. _R News_, *7*(2), 47-52. <URL: https://cran.r-project.org/doc/Rnews/>.

Ekdale, E.G. (2015). Form and function of the mammalian inner ear. J. Anat. 228, pp324—337. DOI: 10.1111/joa.12308

Exdale, E. G. (2013). Comparative Anatomy of the Bony Labyrinth (Inner Ear) of Placental Mammals. PLoS ONE 8(6): e66624. doi:10.1371/journal.pone.0066624

Fish, J. L. (2019). Evolvability of the vertebrate craniofacial skeleton. Semin Cell Dev Biol. July; 91: 13–22. doi: 10.1016/j.semcdb.2017.12.004.

Gerstein, E. R., Gerstein, L., Forsythe, S. E., Blue, J. E. (1999). The underwater audiogram of the West Indian manatee (Trichechus manatus). J. Acoust. Soc. Am. 105 (6)

Gonzales, L. A., Malinzak, M. D., Kay, R. F. (2019). Intraspecific variation in semicircular canal morphology—A missing element in adaptive scenarios? American Journal of Physical Anthropology, 168(1), 10– 24. https://doi.org/10.1002/ajpa.23692

Gunz, P., Ramsier, M., Kuhrig, M. Hublin, J., Spoor, F. (2012). The mammalian bony labyrinth reconsidered, introducing a comprehensive geometric morphometric approach. J. Anat. (2012) 220, pp529–543. doi: 10.1111/j.1469-7580.2012.01493.x

Hackathon, R. et al. (2020). phylobase: Base Package for Phylogenetic Structures and Comparative Data. R package version 0.8.10. https://CRAN.R-project.org/package=phylobase

Hansen, T. F. (2003). Is modularity necessary for evolvability? Remarks on the relationship between pleiotropy and evolvability. BioSystems 69 83–94

Hansen, T. F., Houle, D. (2008). Measuring and comparing evolvability and constraint in multivariate characters. J. EVOL. BIOL. 21. 1201–1219. doi:10.1111/j.1420-9101.2008.01573.x

Hansen, T.F., Houle, D. (2008). Measuring and comparing evolvability and constraint in multivariate characters. J. EVOL. BI O L. 21, 1201–1219. doi:10.1111/j.1420-9101.2008.01573.x

Jombart, T., Dray S. (2008). adephylo: exploratory analyses for the phylogenetic comparative method.

Jones, K.E., Bielby, J., Cardillo, M., Fritz, S.A., O'Dell, J., Orme, C.D.L., Safi, K., Sechrest, W., Boakes, E.H., Carbone, C., Connolly, C., Cutts, M.J., Foster, J.K., Grenyer, R., Habib, M., Plaster, C.A., Price, S.A., Rigby, E.A., Rist, J., Teacher, A., Bininda-Emonds, O.R.P.,

Gittleman, J.L., Mace, G.M. and Purvis, A. (2009). PanTHERIA: a species-level database of life history, ecology, and geography of extant and recently extinct mammals. Ecology, 90: 2648-2648. https://doi.org/10.1890/08-1494.1

Kembel, S. W., Cowan, P.D., Helmus, M.R., Cornwell, W.K., Morlon, H. , Ackerly, D.D. , Blomberg, S.P. , and Webb, C.O. (2010). Picante: R tools for integrating phylogenies and ecology. Bioinformatics 26:1463-1464.

Kirschner, M., Gerhart, J. (1998). Evolvability. Proc. Natl. Acad. Sci. USA Vol. 95, pp. 8420–8427

Köppl, C., Manley, G.A. (2019). A Functional Perspective on the Evolution of the Cochlea. Cold Spring Harb Perspect Med 2019, 9:a033241

Lautenschlager, S., Gill, P., Luo, Z., Fagan M. J., Rayfield E.J. (2017). Morphological evolution of the mammalian jaw adductor complex. Biol. Rev., 92, pp. 1910–1940. 1910. doi: 10.1111/brv.12314

Le Maître, A., Grunstra, N. D. S., Pfaff, C., Mitteroecker, P. (2020). Evolution of the Mammalian Ear: An Evolvability Hypothesis. Evolutionary Biology 47:187–192. doi: 10.1007/s11692-020-09502-0

Liland, K.H., Mevik, B. H., and Wehrens, R. (2022). pls: Partial Least Squares and Principal Component Regression. R package version 2.8-1. https://CRAN.R-project.org/package=pls

Manley, G. A. (2012). Evolutionary paths to mammalian cochleae. Journal of the Association for Research in Otolaryngology, 13(6), 733–743.

Mao, F., Hu, Y., Li, C., Wang, Y., Hill Chase, M., Smith A. K., Meng, J. (2019). Integrated hearing and chewing modules decoupled in a Cretaceous stem therian mammal. Science 367 (6475), 305-308. doi: 10.1126/science.aay9220

Manoussaki, D., Chadwick, R. S., Ketten, D. R., Arruda, J., Dimitriadis, E. K., O'Malley, J. T. (2008). The influence of cochlear shape on low-frequency hearing. PNAS 6162–6166 vol. 105, no. 16

Mitteroecker, P. (2009). The Developmental Basis of Variational Modularity: Insights from Quantitative Genetics, Morphometrics, and Developmental Biology. Evol Biol (2009) 36:377–385. DOI 10.1007/s11692-009-9075-6

Mitteroecker, P. (2020). Morphometrics in Evolutionary Developmental Biology. Springer Nature Switzerland.

Mitteroecker, P., Gunz, P. (2009). Advances in Geometric Morphometrics. Evol Biol (2009) 36:235–247. DOI 10.1007/s11692-009-9055-x

Mitteroecker, P., Gunz, P., Neubauer, S., Müller G. (2012). How to Explore Morphological Integration in Human Evolution and Development? Evol Biol (2012) 39:536–553. DOI 10.1007/s11692-012-9178-3

Mitteroecker, P., Gunz, P., Windhager, S., Schaefer, K. (2013). A brief review of shape, form, and allometry in geometric morphometrics, with applications to human facial morphology. doi:10.4404/hystrix-24.1-6369

Mitteroecker, P., Schaefer, K. (2021). Thirty years of geometric morphometrics: Achievements, challenges, and the ongoing quest for biological meaningfulness. Yearbook Biol Anthropol. 2022; 178 (Suppl. 74): 181–210. doi: 10.1002/ajpa.24531

Murdoch, D., and Adler, D., (2022). rgl: 3D Visualization Using OpenGL. R package version 0.109.6. https://CRAN.R-project.org/package=rgl

Nikaido, M., Nishihara, H., Hukumoto, Y., Okada N. (2003). Ancient SINEs from African Endemic Mammals. Mol. Biol. Evol. 20(4):522–527. doi: 10.1093/molbev/msg052

Navarro-Díaz, A., Esteve-Altava, B., Rasskin-Gutman, D. (2019). Disconnecting bones within the jaw-otic network modules underlies mammalian middle ear evolution. J. Anat. 235, pp15—33. doi: 10.1111/joa.12992

Orme, D., Freckleton, R., Thomas, G., Petzoldt, T., Fritz, S., Isaac N., and Pearse, W. (2018). caper: Comparative Analyses of Phylogenetics and Evolution in R. R package version 1.0.1. https://CRAN.R-project.org/package=caper

Paradis, E., Schliep, K. (2019). ape 5.0: an environment for modern phylogenetics and evolutionary analyses in R. Bioinformatics 35: 526-528.

Pavlicev, M., Hansen, T. F. (2011), Genotype-Phenotype Maps Maximizing Evolvability: Modularity Revisited. Evol Biol 38:371–389. doi:10.1007/s11692-011-9136-5

Pennell, M. W., Eastman, J. M., Slater, G. J., Brown, J. W., Uyeda, J. C., FitzJohn, R. G., Alfaro, M.E., and Harmon, L. J. (2014). geiger v2.0: an expanded suite of methods for fitting macroevolutionary models to phylogenetic trees. Bioinformatics 30:2216-2218.

R Core Team (2021). R: A language and environment for statistical computing. R Foundation for Statistical Computing, Vienna, Austria. URL https://www.R-project.org/.

Revell, L. J. (2012). phytools: An R package for phylogenetic comparative biology (and other things). Methods Ecol. Evol. 3 217-223. doi:10.1111/j.2041-210X.2011.00169.x

Riedl, R. J. (1978). Order in Living Organisms. New York: John Wiley and Sons.

Rohlf, F.J., Corti, M., (2000). Use of Two-Block Partial Least-Squares to Study Covariation in Shape. Syst. Biol. 49(4):740–753

Rohlf, F. J., Slice, D., (1990). Extensions of The Procrustes Method For The Optimal Superimposition of Landmarks. Syst. Zool., 39(1):40-59

RStudio Team (2022). RStudio: Integrated Development Environment for R. RStudio, PBC, Boston, MA URL http://www.rstudio.com/.

Sauerland, M., Dehnhardt, G., (1998). Underwater audiogram of a tucuxi (Sotalia fluviatilis guianensis). J. Acoust. Soc. Am. 103 (2), February 1998

Schauberger, P. and Walker, A. (2021). openxlsx: Read, Write and Edit xlsx Files. R package version 4.2.5. https://CRAN.R-project.org/package=openxlsx

Schlager, S. (2017). Morpho and Rvcg - Shape Analysis in R. In Zheng G, Li S, Szekely G (eds.), _Statistical Shape and Deformation Analysis_, 217-256. Academic Press. ISBN 9780128104934.

Silcox, M.T., Blocj, K. T., Boyer, D. M., Godinot, M., Ryan, T. M., Spoor, F., Walker, A. (2009). Semicircular canal in early primates. Journal of Human Evolution 56 315–327. doi:10.1016/j.jhevol.2008.10.007

Slowikowski, K. (2021). ggrepel: Automatically Position Non-Overlapping Text Labels with 'ggplot2'. R package version 0.9.1. https://CRAN.R-project.org/package=ggrepel

Spoor, F., Garland, T., Krovitz, G., Ryan, T. M., Silcox, M. T., & Walker, A. (2007). The primate semicircular canal system and locomotion. Proceedings of the National Academy of Sciences, 104(26), 10808–10812. doi:10.1073/pnas.0704250104

Tabuce, T., Asher, R. J., Lehmann, T. (2008). Afrotherian mammals: a review of current data. Mammalia 72 (2008): 2–14. DOI: 10.1515/MAMM.2008.004

Thioulouse, J., Dray, S., Dufour, A., Siberchicot, A., Jombart, T., Pavoine, S. (2018). _Multivariate Analysis of Ecological Data with ade4_. Springer. doi: 10.1007/978-1-4939-8850-1 (URL: https://doi.org/10.1007/978-1-4939-8850-1).

Urbanek, S., (2021). jpeg: Read and write JPEG images. R package version 0.1-9. https://CRAN.R-project.org/package=jpeg

Wagner, G. P., Altenberg, L. (1996). Complex Adaptations and the Evolution of Evolvability. Evolution, 50(3), pp. 967-976

Wartzok, D., Ketten, D.R. (1999). Marine Mammal Sensory Systems. Biology of Marine Mammals. J. Reynolds and S. Rommel (eds.), Smithsonian Institution Press, 1999, pp. 117-175.

West, C. D. (1985). The relationship of the spiral turns of the cochlea and the length of the basilar membrane to the range of audible frequencies in ground dwelling mammals. J. Acoust. Soc. Am. 77 (3)

Wickham, H. (2016). ggplot2: Elegant Graphics for Data Analysis. Springer-Verlag New York

Wickham, H. (2022). forcats: Tools for Working with Categorical Variables (Factors). R package version 0.5.2. https://CRAN.R-project.org/package=forcats

Wickham, H. and Bryan, J. (2022). readxl: Read Excel Files. R package version 1.4.0. https://CRAN.R-project.org/package=readxl

Wilson, D. E., Mittermeier, R. A., and Cavallini, P. (2009). Handbook of the mammals of the world (Volumes 1, 2, 4, 5, 6, 7, 8, 9). Lynx Edicions: Conservation International: IUCN.

Yihui, X. (2022). knitr: A General-Purpose Package for Dynamic Report Generation in R. R package version 1.39.

Appendix

Detailed List of Specimens and their Sources

Scientific Name	"Supra-ordinal" Taxon	"Order"	Source[1]	Catalog no.	Sex	Side
Amblysomus hottentotus	Afrotheria	Afrosoricida	MCZ	mcz:mamm:57045	M	R
Chrysochloris asiatica	Afrotheria	Afrosoricida	MVZ	mvz:mamm:183379	U	L
Hemicentetes semispinosus	Afrotheria	Afrosoricida	YPM	ypm mam 005783	U	R
Limnogale mergulus	Afrotheria	Afrosoricida	MCZ	mcz:mamm:45533	F	L
Oryzorictes tetradactylus	Afrotheria	Afrosoricida	NHMW	NMW_948	U	L
Potamogale velox	Afrotheria	Afrosoricida	NHMW	NMW_3329	U	L
Setifer setosus	Afrotheria	Afrosoricida	DU	du:ea:037	U	R
Tenrec ecaudatus	Afrotheria	Afrosoricida	YPM	ypm mam 006029	U	R
Dendrohyrax arboreus	Afrotheria	Hyracoidea	NHMW	NMW_42313	M	R
Heterohyrax brucei	Afrotheria	Hyracoidea	NHMW	NMW_20087	U	R
Procavia capensis	Afrotheria	Hyracoidea	UMZC	umzc:H4981C	M	L
Elephantulus rufescens pulcher	Afrotheria	Macroscelidea	MCZ	mcz:mamm:57173	M	R
Elephantulus rupestris jamesoni	Afrotheria	Macroscelidea	MVZ	mvz:mamm:117069	M	L
Macroscelides proboscideus	Afrotheria	Macroscelidea	NHMW	NMW_48465	F	L
Petrodromus tetradactylus	Afrotheria	Macroscelidea	CAS	cas:mam:28177	F	R
Rhynchocyon stuhlmanni	Afrotheria	Macroscelidea	NHMW	NMW_8897	F	R
Elephas maximus	Afrotheria	Proboscidea	NHMW	NMW_2526	U	L
Dugong dugon	Afrotheria	Sirenia	NHMW	NMW_7548	U	R
Trichechus sp.	Afrotheria	Sirenia	NHMW	NMW_75597	U	L
Orycteropus afer faradjius	Afrotheria	Tubulidentata	AMNH	m-51909	F	R
Ochotona rufescens	Euarchonto-glires	Lagomorpha	NHMW	NMW_59746	U	L
Oryctolagus cuniculus	Euarchonto-glires	Lagomorpha	IUPW	IUPW_LB_5	U	L
Marmota marmota	Euarchonto-glires	Rodentia	IUPW	IUPW_697	U	R

Mus musculus	Euarchonto-glires	Rodentia	NHMW	NMW_66775	F	R
Rattus rattus	Euarchonto-glires	Rodentia	NHMW	NMW_24077	U	L
Cryptomys hottentotus	Euarchoto-glires	Rodentia	NHMW	NMW_26144	U	R
Microtus arvalis	Euarchoto-gliresn	Rodentia	NHMW	NMW_40451	U	L
Tragulus javanicus	Laurasiatheria	Artiodactyla	NHMW	NMW_40820	M	L
Lutra lutra	Laurasiatheria	Carnivora	NHMW	NMW_61316	F	R
Odobenus rosmarus	Laurasiatheria	Carnivora	NHMW	NMW_4036	F	L
Phoca vitulina	Laurasiatheria	Carnivora	NHMW	NMW_1457	M	R
Sotalia fluviatilis	Laurasiatheria	Cetartio-dactyla	NHMW	NMW_75400	U	R
Erinaceus europaeus	Laurasiatheria	Eulipotyphla	LACM	lacm:mammals:058376	M	R
Sorex araneus	Laurasiatheria	Eulipotyphla	NHMW	NMW_57583	M	L
Talpa europaea	Laurasiatheria	Eulipotyphla	IUPW	IUPW_1666	U	L
Manis tricuspis	Laurasiatheria	Pholidota	NHMW	NMW_15230	M	R
Didelphis sp.	Marsupialia	Didelphi-morphia	TMM	tmm:m:2517	M	R
Ornithorhynchus anatinus	Monotremata	Monotremata	NHMW	NMW_2028	M	R
Tolypeutes matacus	Xenarthra	Cingulata	NHMW	NMW_75964	M	R
Tamandua mexicana	Xenarthra	Pilosa	NHMW	NMW_31568	F	R

[1] Specimens from the NHM Vienna were micro-CT scanned for the purpose of this study, whereas the other specimens had already been scanned in the context of other projects by a collaborator (Cathrin Pfaff) or by colleagues in the broader scientific community (MorphoSource).

Contextual Data

Common Name	Body Mass (g)	Pursue Moving Prev	Aquatic	Arboreal	Ground Dwelling	Scansorial	Cursorial	Hopping	Jumping	Leaping	Fossorial	3D Movementnt	Agility	Orthogrady vs. Pronogrady	Foot Position
Ambly-somus hottentotus	62,6	1	1	1	1	1	1	1			3	1	2	5	1
Chryso-chloris asiatica	37,16	1	1	1	2	1	1	1			3	1	2	5	1
Cryptomys hottentotus	75,13	1	1	1	1	1	1	1			3	1	2	5	1
Dendro-hyrax arboreus	2981,11	1	1	3	2	3	2	1			1	3	4	5	2
Didelphis sp	1428	2	1	2	2	2	1	1			1	2	3	5	1
Dugong dugon	295000	1	4	1	1	1	1	1			1	3	1	3	n/a
Elephan-tulus rufescens	52,78	2	1	1	3	1	2	1			1	1	5	5	3
Elephan-tulus rupestris	65,56	2	1	1	3	2	2	1			1	2	5	5	3
Elephas maximus	3269794	1	1	1	3	1	1	1			1	1	2	4	1
Erinaceus europaeus	777,95	1	1	1	3	2	2	1			2	2	3	5	3
Hemicent-etes semi-spinosus	134	1	1	1	2	1	1	1			3	1	3	5	1
Heterohyrax brucei	2453,66	1	1	2	2	3	2	2			1	3	4	5	2
Limnogale mergulus	76,86	2	3	1	2	1	1	1			2	3	4	5	1
Lutra lutra	8868,69	3	2	1	2	1	2	2			2	2	5	4	1
Macro-scelides probo-scideus	38,64	2	1	1	3	1	2	1			2	1	5	5	3
Manis tricuspis	1539,31	1	1	2	2	3	1	1			1	2	2	4	1
Marmota marmota	4059,15	1	1	1	3	1	2	1			2	1	4	4	1
Microtus arvalis	26,9	1	1	1	3	1	2	1			3	1	4	5	1

Mus musculus	19,3	1	1	1	3	2	2	1	1	2	4	5	1
Ochotona rufescens	250	1	1	1	3	1	1	3	2	2	5	5	2
Odobenus rosmarus	1042996	1	3	1	2	1	1	1	1	3	3	3	n/a
Ornithor-hynchus anatinus	1484,25	2	3	1	2	1	1	1	2	3	4	3	1
Orycteropus afer faradjius	56175,2	1	1	1	3	1	1	1	2	1	4	4	3
Oryctolagus cuniculus	1590,57	1	1	1	3	1	2	3	2	2	6	4	2
Oryzorictes tetra-dactylus	35,99	1	1	1	2	1	1	1	3	1	3	5	1
Petro-dromus tetra-dactylus	201	2	1	1	3	1	2	1	1	1	5	5	3
Phoca vitulina	87316,66	3	3	1	2	1	1	1	1	3	5	3	n/a
Potamogale velox	670,99	2	2	1	2	1	1	1	2	2	5	4	1
Procavia capensis	2952,48	1	1	2	3	2	2	2	1	3	4	5	2
Rattus rattus	142,68	2	1	2	3	2	2	1	2	3	4	5	1
Rhyncho-cyon cirnei	424,92	2	1	1	3	1	2	1	1	1	5	5	3
Setifer setosus	263,22	1	1	2	3	2	1	1	2	1	3	5	1
Sorex araneus	9,18	1	1	1	3	1	1	1	2	1	4	5	1
Sotalia fluviatilis	42833,44	3	4	1	1	1	1	1	1	3	5	3	n/a
Talpa europaea	87,53	1	1	1	1	1	1	1	3	1	2	5	1
Tamandua mexicana	4178,51	1	1	2	2	3	1	1	1	3	3	4	1
Tenrec ecaudatus	887,59	1	1	1	3	2	1	1	2	1	4	5	1
Tolypeutes matacus	1303,47	1	1	1	3	1	2	1	2	1	3	5	3
Tragulus javanicus	1889,93	1	1	1	3	1	1	1	2	1	4	5	4
Trichechus sp	446442	1	4	1	1	1	1	1	1	3	1	3	n/a